LRP 502/94 September 1994

STABILIZATION OF IDEAL MODES BY RESISTIVE WALLS IN TOKAMAKS WITH PLASMA ROTATION AND ITS EFFECT ON THE BETA LIMIT

D.J. Ward and A. Bondeson

submitted for publication in

PHYSICS OF PLASMAS

STABILIZATION OF IDEAL MODES BY RESISTIVE WALLS IN TOKAMAKS WITH PLASMA ROTATION AND ITS EFFECT ON THE BETA LIMIT

D. J. Ward[a] and A. Bondeson[a,b]

[a]Centre de Recherches en Physique des Plasmas, Association Euratom–Confédération Suisse, Ecole Polytechnique Fédérale de Lausanne, 1007 Lausanne, Switzerland

[b]Department of Technology, Euratom-NFR Association, Uppsala University, Box 534, S-751 21 Uppsala, Sweden

Abstract

It is shown that pressure-driven, ideal external modes in tokamaks can be fully stabilized by resistive walls when the plasma rotates at some fraction of the sound speed. For wall stabilized plasmas, there are two types of potentially unstable external modes: those which are nearly locked to the wall and those which rotate with the plasma. For the modes rotating with the plasma, the stabilizing effect of the wall increases when the wall is brought closer to the plasma, while, for the wall-locked modes, the stabilization improves with *increasing* wall distance. When the plasma rotates at some fraction of the sound speed, there is a window of stability to both the wall-locked and the rotating mode. This window closes when beta exceeds a new limit which can be significantly higher than the wall-at-infinity limit. The stabilization depends principally on the toroidal coupling to sound waves and is affected by ion Landau damping. Two dimensional stability calculations are presented to evaluate the gains in beta limit resulting from this wall stabilization for different equilibria and rotation speeds. In particular, results are shown for advanced tokamak configurations with bootstrap fractions of $\approx 100\%$.

PACS numbers: 52.35.Py, 52.30.-q, 52.55.Fa, 52.35.Dm

I. Introduction

An important limit to tokamak performance is that of the ratio, beta, of the particle pressure to the magnetic field pressure, $\beta = 2\mu_0\langle p\rangle/\langle B^2\rangle$, where $\langle\cdots\rangle$ denotes volume average. Large values of beta are desirable, because in a reactor the fusion efficiency scales with beta as does the ignition parameter. An upper limit to beta is set by ideal MHD instabilities, which can cause a rapid termination of the discharge. Troyon et al.[1] found numerically that the beta limit is proportional to the plasma current I_p, $\beta_{\max} = gI_p[\mathrm{MA}]/a[\mathrm{m}]B_0[\mathrm{T}]$, where a is the minor radius and B_0 is the magnetic field on axis. This scaling has since been well confirmed experimentally and in other numerical studies, although rather different normalized betas, g, have been achieved in different tokamaks.

Beta limits are normally computed by requiring ideal MHD stability of static equilibria without accounting for any stabilization by conducting walls. Early computations[1] gave $g \approx 2.8$, and subsequent studies, where the profiles were further optimized, have yielded higher estimates of g; up to 3.5 or 4. (A review of tokamak stability at high beta has been given recently by Strait.[2]) However, experimental work on the DIII-D tokamak[3] has achieved $g \approx 5$, and MHD stability analyses show that at least some of these discharges are unstable to modes of low toroidal mode number n with the wall at infinity. These same cases have been shown to be stable with an ideal conducting wall at the position of the DIII-D vacuum vessel.[4]

Since the pressure limit is set by robust, global instabilities, kinetic corrections due to drift frequencies, finite Larmor radii or trapped particles can be estimated to be small. Conventional wisdom[5] holds that ideal MHD instabilities are only slowed down, but never completely stabilized, by resistive walls. It has been suggested[6] that such modes might be stabilized by rotation of the plasma within a resistive wall, and, in fact, the high beta DIII-D discharges are usually rotating due to unbalanced neutral beams.[4] We present here theoretical results that show that these pressure driven external modes can be completely

stabilized by resistive walls and toroidal rotation of the plasma. The gain in confined pressure due to this stabilizing effect can be significant. Part of this work has been presented elsewhere.[7]

It is well established that resistive walls do not change the stability boundaries of the axisymmetric "vertical" instability[8] and the "cylindrical" external kink mode,[9,10] when the plasma has no resonant surface where $k_{\|} \equiv (m/q - n)/R_0$ vanishes (m = poloidal mode number, q = safety factor and R_0 = major radius). Resistive walls slow down the growth of these instabilities to the resistive time of the wall, $\tau_w = L/R$, but do not change the stability boundary from their wall-at-infinity value. Furthermore, the growth rates of these modes are not affected by sub-Alfvénic plasma rotation.[8–10]

By contrast, tearing modes can be wall-stabilized in the presence of rotation provided the rotation frequency exceeds both τ_w^{-1} and a characteristic tearing growth rate.[9,11,12] This type of stabilization was recently put forward by Finn[13] as an explanation of the DIII-D results,[4] although no convincing argument was given for how rotation on the *resistive*-MHD time scale would stabilize an *ideal* instability.

Generally, the stability boundary is not changed by resistive walls and plasma rotation when the rotation frequency remains small compared with the local Alfvén frequency $k_{\|} v_A$ throughout the plasma. This condition is clearly violated by the toroidal pressure-driven external kink modes for which $k_{\|}$ vanishes locally at the resonant surfaces where $m = nq$. Evidently, there will be layers around each resonant surface where the rotation frequency exceeds the local Alfvén frequency and where the plasma response to a wall locked mode is dominated by inertia. Furthermore, for pressure driven modes the parallel motion is important and this is influenced by inertia when the rotation is comparable to the sound speed.

II. Calculation

The toroidal pressure driven modes are more complicated than the cylindrical tearing mode because of the toroidal coupling between different poloidal harmonics and between the Alfvén and sound waves. Therefore, we have used numerical computation to study the effect of resistive wall stabilization with rotation in toroidal geometry. The spectral codes MARS[14] and NOVA[15,16] have been modified to include a resistive shell in the vacuum region surrounding the plasma. As a minimum modification to existing toroidal stability codes, we have modeled rigid plasma rotation by making the resistive shell rotate rather than the plasma. Thus, the equilibrium is static, which allows us to separate the effects of wall stabilization from other modifications due to the plasma rotation. In most calculations reported here, the rotation frequency is much larger than any resistive growth rate so that the plasma can be treated as ideally conducting (this excludes resistive modes rotating with the plasma).

A. Resistive Wall

Both codes use a thin resistive wall model which divides the vacuum surrounding the plasma into two distinct regions. The two regions are connected by the boundary condition at the resistive wall, which includes the effect of toroidal rotation of the resistive wall boundary. Faraday's law is combined with Ohm's law (including the toroidal velocity of the wall) to give a boundary condition that relates the components of the magnetic field across the resistive wall.

The NOVA-W[15] code uses a Green's function technique that is a modification of the ideal calculation.[16] In this model, the perturbed magnetic field in the vacuum is represented by the gradient of a scalar potential, $\vec{b} = \nabla\Phi$. The effect of the thin resistive wall enters

as a jump in the scalar potential across the wall:

$$\Delta\Phi = \Phi_{\text{out}} - \Phi_{\text{in}} \tag{1}$$

This is then related to the normal derivative of the potential $(\hat{n} \cdot \nabla\Phi)$ at the wall through the boundary condition:

$$i(\omega - n\omega_{\text{rot}})(\hat{n} \cdot \nabla\Phi) = -n^2 \frac{\eta}{\delta} \frac{\Delta\Phi}{R^2} + \frac{1}{R(R_\theta^2 + Z_\theta^2)} \frac{\partial}{\partial\theta} \left(\frac{\eta}{\delta} \frac{R}{R_\theta^2 + Z_\theta^2} \frac{\partial \Delta\Phi}{\partial\theta} \right) \tag{2}$$

Here $\eta(\theta)$ is the wall resistivity, and $\delta(\theta)$ is its thickness, R and Z are the coordinates of the wall contour in a (R, ϕ, Z) cylindrical coordinate system, $R_\theta = \partial R/\partial\theta$ (the derivative in the poloidal angle), and ω_{rot} is the rotation velocity of the wall.

In calculating the vacuum boundary condition, the MARS code uses a discretized vacuum inside and outside the resistive shell. The perturbed magnetic field in those two regions satisfies the conditions:

$$\nabla \cdot \vec{b} = 0 \qquad \& \qquad \nabla \times \vec{b} = 0 \tag{3}$$

In MARS, the magnetic field is represented as

$$\vec{b} = b^1 \nabla\theta \times \nabla\phi + b^2 \nabla\phi \times \nabla s + b^3 \nabla s \times \nabla\theta \tag{4}$$

where s is the coordinate labeling the poloidal flux surfaces. The boundary condition at the resistive shell that relates the normal and tangential components b^1 and b^2, respectively, is similar in form to the boundary condition in Eq. (2):

$$i(\omega - n\omega_{\text{rot}})b^1 = \frac{d}{\tau_w} \left(|\nabla s| \Delta \frac{\partial b^1}{\partial s} - 2\Delta b^2 \frac{\partial}{\partial\theta} |\nabla s| \right) \tag{5}$$

Here, d is the wall radius on the midplane and τ_w is the resistive wall time constant.

B. Sound Wave Damping

Sonic rotation complicates the stability problem by coupling to sound waves, and it has been pointed out that the MHD equations predict an unphysical resonant behavior of

the sound waves.[17] For realistic temperature ratios, the sound waves are strongly damped by ion Landau damping, and an accurate calculation requires a description that is kinetic along the field lines. However, reasonable approximations of the kinetic behavior can be obtained by adding dissipative terms to the fluid equations.[18] We have applied three such modifications of the scalar pressure, ideal MHD equations. Two of these consist of adding a damping term for the Lagrangian pressure perturbations. The perturbed pressure is split into a convective and a Lagrangian part,

$$p_1 = -\vec{\xi} \cdot \nabla p_0 + p_{1L} \tag{6}$$

where

$$\partial p_{1L}/\partial t = -\Gamma p_0 \nabla \cdot \vec{v} - \nu p_{1L} \tag{7}$$

The damping rate ν is either taken to be a fixed number or to represent a thermal diffusivity following the Hammett-Perkins[18] approximation, $\nu = \chi |k_\parallel v_{\rm thi}|$. As a third alternative, we use a term representing parallel viscosity in the equation of motion along the field lines so that $v_\parallel \equiv (\vec{B}_0/B_0) \cdot \vec{v}$ is computed from

$$\partial v_\parallel/\partial t = -(\vec{B} \cdot \nabla p)_1/B_0\rho_0 - \kappa |k_\parallel v_{\rm thi}| v_\parallel \tag{8}$$

By comparison with the guiding center results in Ref. 17, one can show that this formulation with $\Gamma = 3/2$, $\kappa = \sqrt{\pi} \approx 1.77$ and $\nu = 0$ gives a good approximation for the perturbed perpendicular pressure induced by Lagrangian perturbations of the magnetic field strength.

III. Resistive Wall and Plasma Modes

We now present results from numerical solutions of the MHD eigenvalue problem modified according to Eq. (7) or Eq. (8). The resistive shell rotates toroidally with the angular frequency $\omega_{\rm rot}$, and its time constant τ_w is long compared with ideal MHD time scales and

$\omega_{\rm rot}^{-1}$. Using the MARS and NOVA codes, we search for eigenvalues in the complex plane, giving the growth rate and the rotation frequency of the mode with respect to the wall.

Figure 1 shows a typical example of how the growth rate varies with respect to the wall position. The growth rate, $\gamma_{\rm res}$, and the slip frequency, $\Delta\omega_{\rm res} = \omega_{\rm rot} - \omega_{\rm res}$ (rotation frequency minus the mode rotation frequency), both normalized to the wall time, are shown as functions of the wall position. Also shown is the normalized ideal growth rate for a wall located outside the marginal position of an ideally conducting wall.

When the pressure exceeds the stability limit with the wall at infinity, we find two classes of modes that can potentially be unstable: (a) one which has zero frequency in the frame of the plasma and hardly penetrates the resistive wall: the "plasma mode," and (b) one which penetrates the wall and rotates slowly with respect to it (slip frequency, $\Delta\omega_{\rm res} = O(\tau_w^{-1}) \ll \omega_{\rm rot}$): the "resistive wall mode". The resistive wall mode rotates with respect to the plasma at a frequency close to the imposed rotation frequency $\omega_{\rm rot}$. The two modes are influenced in opposite ways by the wall distance—the plasma mode is *destabilized* as the wall is moved further from the plasma, while the resistive wall mode is *stabilized.*

The plasma mode rotates quickly (frequency $\approx \omega_{\rm rot} \gg \tau_w^{-1}$) with respect to the wall. It does not penetrate the wall and behaves as if the wall were ideal. The plasma mode is unstable on the ideal MHD time scale when the wall radius exceeds the usual ideal MHD threshold for wall stabilization, $d_{\rm ideal}$. This marginal wall position approaches infinity at the conventional beta limit and decreases with increasing pressure.

The resistive wall mode, on the other hand, becomes increasingly stable as the resistive wall is moved away from the plasma. It becomes completely stable at some threshold position, and it remains stable for all wall positions outside this threshold. Therefore, there can be a finite window for the wall position such that *both* the plasma and the resistive wall modes are stable. If the wall is moved outside this region closer to the plasma, the resistive wall mode will become unstable, whereas if it is moved further from the plasma

the ideal mode will become unstable.

A. Large-Aspect-Ratio Calculation of Δ' at the Wall

This counter-intuitive effect of the wall position on the stability of the resistive wall mode can be understood from a large-aspect-ratio calculation of Δ' at the resistive shell. We consider a magnetic perturbation in the vacuum, dominated by one poloidal harmonic m (assumed to be positive). The perturbed magnetic flux function ψ satisfies $\nabla_\perp^2 \psi = 0$ in the vacuum region and the solution the vacuum region inside the resistive wall is given by

$$\psi_- = c_1 r^{-m} + c_2 r^m \tag{9}$$

and the solution in region outside the resistive wall (extending to infinity) is:

$$\psi_+ = c_3 r^{-m} \tag{10}$$

The resistive shell is at $r = d$, and the growth rate of the resistive wall mode is given by $\gamma = \tau_w^{-1} d\Delta'_w$, where $\Delta'_w = [\psi'(d_+) - \psi'(d_-)]/\psi(d)$. We can write the logarithmic derivative of ψ at the plasma edge, $r = a$, as

$$\left(\frac{\psi'}{\psi}\right)_{r=a} = -\frac{m}{a}(1+z) \tag{11}$$

with $z = x + iy$, x and y real. For static equilibria, the imaginary part y vanishes, but in the presence of rotation, y is forced to be nonzero (if there is at least one resonance where $\omega_{\rm rot}$ equals the frequency of the coupled Alfvén-sound continuum).

By applying continuity of ψ at the resistive wall, we can eliminate one of the three unknown constants c_k, and applying the boundary condition at the plasma boundary, Eq. (11), eliminates a second. This gives for Δ'_w:

$$\Delta'_w \frac{d}{2m}[1 - (a/d)^{2m}] = \frac{z}{(w-z)} = \frac{(wx - x^2 - y^2) + iwy}{(w-x)^2 + y^2} \tag{12}$$

where $w = 2/[(d/a)^{2m} - 1]$ is a geometric factor representing the wall position. As the radius of the resistive shell d increases from the plasma radius, $d = a$, to $d \to +\infty$, w *decreases* from infinity to 0.

Let us first consider the case of no rotation, $y = 0$, and the plasma unstable in the absence of a wall, $x > 0$. For this case, Eq. (12) shows that the resistive wall mode is unstable ($\Delta'_w > 0$) for $w > x$, or equivalently, for $a \leq d < d_{\text{ideal}} \equiv a(1 + 2/x)^{1/2m}$. As the wall radius increases, $\Delta'_w \to \infty$ when $d \to d_{\text{ideal}}$, (which corresponds to $w = x$) and at this wall position, the resistive wall mode connects to the ideal MHD instability, which is unstable for $d > d_{\text{ideal}}$. In the region of ideal instability, plasma inertia is non negligible and modifies $(\psi'/\psi)_{r=a}$ so as to keep $\Delta'_w \approx +\infty$ for $d > d_{\text{ideal}}$.

When there is rotation, the logarithmic derivative has a nonzero imaginary part, y. This eliminates the zero in the denominator of Eq. (12). Consequently, Δ'_w remains finite and complex for all wall distances, and the resistive wall mode does not connect to the ideal instability. Thus, rotation effectively separates the resistive wall mode from the plasma mode for all values of d. The growth rate of the resistive wall mode remains $O(\tau_w^{-1})$ for all d, and if $\tau_w \gg \tau_A$, the plasma response can be computed neglecting the small slip frequency with respect to the wall. (These conclusions are dependent on the assumption that $(\psi'/\psi)_{r=a}$ is independent of the $O(\tau_w^{-1})$ growth rate, which, of course, fails if $\omega_{\text{rot}}\tau_w$ is order one or less.) Furthermore, because of the damping added to the sound waves and the toroidal coupling of sound and Alfvén waves, the solution in the plasma remains well behaved as $\text{Re}(\gamma) \to 0$, i.e., the continuum resonances of the ideal MHD equations have moved into the stable half plane.

When there is no rotation, $y = 0$, and the resistive wall mode is unstable for all values of wall radius d. At $d = d_{\text{ideal}}$ it connects to the ideal mode. However, Eq. (12) shows that rotation, through the nonzero magnitude of y, is stabilizing. The resistive wall mode is stabilized as $\text{Re}(\Delta'_w) \to 0$. This occurs as the geometric factor w decreases, or, equivalently, as the wall radius d *increases*. Figure 1 shows that the resistive wall mode is stabilized

when d exceeds a threshold, which, according to Eq. (12), is given by $wx = x^2 + y^2$ which gives the marginally stable wall position:

$$d_{\rm res} = a\left(1 + \frac{2x}{(x^2+y^2)}\right)^{1/2m} \tag{13}$$

The resistive wall mode remains stable when $wx > x^2 + y^2$, i.e. when $d > d_{\rm res}$.

Although the present discussion is oversimplified, e.g., by only considering one poloidal harmonic, it demonstrates two important aspects of the behavior of resistive wall modes: (1) the plasma and resistive wall modes are separated by rotation that is rapid compared with the wall time (and resistive MHD times[9,11,13]), and (2) they behave in opposite ways with respect to the wall distance. These two conclusions are ultimately due to the nonzero value of the imaginary component of $(\psi'/\psi)_{r=a}$, when there is rotation. It is clear that the optimum wall position lies within the region stable to both the resistive wall mode and the ideal mode, and it is some distance away from the plasma.

We conclude that, when a rotating plasma exceeds the pressure limit for low-n stability with the wall at infinity, there are two stability limits for the wall radius, $d_{\rm res}$ and $d_{\rm ideal}$. The plasma is stable when $d_{\rm res} < d < d_{\rm ideal}$, and this condition must apply for all n (except $n = 0$ which is usually stabilized by active feedback on the resistive wall time scale).

B. Equilibria in the First Stability Region

We have computed stability limits including rotation and resistive walls for several MHD equilibria. Generally, the effect of wall stabilization is stronger when the pressure profile is broad so that the beta limit is set by external modes. An example is given in Fig. 2 which shows $d_{\rm ideal}$ and $d_{\rm res}$ versus normalized pressure g for $n = 1$ and 2 and rotation frequency $|\omega_{\rm rot}/\omega_A| = 0.06$. The computations were made for an equilibrium with JET shape (elongation = 1.7, triangularity = 0.3 and aspect ratio = 3) and a low pressure peaking factor, $p_0/\langle p\rangle \approx 1.7$. The current profile was adjusted to keep the safety factor

at the magnetic axis and at the edge of the plasma fixed: $q_0 = 1.2$ and $q_s = 2.55$. The resistive shell was conformal with the plasma boundary and we used the parallel viscosity model Eq. (8) with $\kappa = 1.77$.

In Fig. 2, d_{ideal} is smaller for $n = 2$ than for $n = 1$, thus the outer stability limit for the wall position is set by $n = 2$ not by $n = 1$. In fact, $n = 3$ gives an even more restrictive d_{ideal}. However, the present model is somewhat unrealistic for high-n modes. First, strong shaping, such as in DIII-D, can cause a transition to second stability for large and intermediate n. Second, experimentally, the plasma is rotating rather than the wall, and the velocity profile in the plasma is sheared, which is expected to stabilize high-n ballooning modes.[19] Thus, the stability boundaries of the high-n and intermediate-n modes should be more sensitive both to the profile of the plasma rotation and to geometrical effects. Although a general conclusion cannot be drawn from the example in Fig. 2, it is clear that the most restrictive d_{ideal} can be set by toroidal mode numbers larger than 1. On the other hand, our computations indicate that the inner limit, d_{res}, is generally set by the $n = 1$ resistive wall mode. An important reason why the present mechanism of wall stabilization influences the overall beta limit is that it is effective for low-n modes, in particular, $n = 1$, for which shaping effects alone are not enough to produce second stability.[20]

For the equilibria in Fig. 2, the highest g-factor that is stable to both $n = 1$ and $n = 2$ at the prescribed rotation frequency is about 4.2, to be compared with the threshold of 3.1 in the absence of wall stabilization. The effect of wall stabilization is strongly profile dependent, not only because of the different effects of the wall on internal or external modes, but also because of the spectrum of n-values that can become unstable.

A considerable uncertainty comes from computing the perturbed pressure from fluid rather than kinetic theory. Figure 3 shows the results of different fluid approximations for the same equilibria as in Fig. 2 with $|\omega_{\text{rot}}/\omega_A| = 0.06$. Stability limits are shown for the $n = 1$ resistive wall mode using the model of Eq. (6) with $\nu/\omega_A = 0.0025$ and $\nu/\omega_A = 0.025$ and the parallel viscosity model. Eq. (8), with $\Gamma = 1.5$ and $\kappa = 1.77$, 0.885

and 0.1. The Hammett-Perkins approximation with $\chi = 2/\pi$ gives a result almost identical to the pressure damping model with $\nu/\omega_A = 0.025$. Thus, the two pressure damping models Eq. (6) give very similar results, while the parallel viscosity model, Eq. (8), gives a somewhat stronger stabilizing effect. Furthermore, if the sound waves are eliminated by setting $\Gamma = 0$, the wall stabilization becomes very weak for $|\omega_{\rm rot}/\omega_A| \leq 0.1$. We conclude that the magnitude of the stabilization by resistive walls and rotation is sensitive to the dynamics of sound waves and an accurate theory must be kinetic along the field lines (e.g., drift kinetic).

Also shown in Fig. 3 is a comparison case with half the rotation frequency, $|\omega_{\rm rot}/\omega_A| = 0.03$ (and $\Gamma = 1.5$, $\kappa = 1.77$). The stabilization is much weaker for this lower rotation frequency and is almost lost when $|\omega_{\rm rot}/\omega_A| \leq 0.02$. Thus, there is a threshold behavior with respect to the rotation frequency. For the type of equilibria we have examined, $|\omega_{\rm rot}/\omega_A|$ needs to be about 0.05 to give a significant stabilizing effect. This corresponds to a minimum rotation frequency of about 20% of the sound frequency at the $q = 2$ surface.

Another example shows the sensitive dependence of the stabilization on the rotation frequency at fixed beta. In Fig. 4 the dependence of growth rate on wall position is shown for several different rotation velocities. The resistive wall growth rate with respect to wall position for the case with no rotation is also shown for comparison. Here an unstable equilibrium similar to those just considered, except with $q_s = 3.55$, with $g = 4.3$ is examined using the constant pressure damping model, Eq. (6), for $\nu/\omega_A = 0.01$. This case shows a strong dependence on $\omega_{\rm rot}$. The lowest value of rotation for which any stabilization is seen is for $|\omega_{\rm rot}/\omega_A| = 0.045$, but only for large values of d/a. Increasing $|\omega_{\rm rot}/\omega_A|$ significantly increases the region of stability by moving the stability threshold value of $d_{\rm res}$ closer to the plasma surface. For high rotation frequencies of $|\omega_{\rm rot}/\omega_A| \geq 0.065$, the resistive wall mode is stabilized for all wall positions. This behavior of $d_{\rm res}$ with respect to $\omega_{\rm rot}$ gives a continuous enlargement of the stability region with increasing rotation starting from a minimum threshold rotation where $d_{\rm res} < d_{\rm ideal}$ to much higher rotation frequencies where

$d_{res} \approx a$.

We find that when q_s is increased, for equilibria with similar pressure profiles, d_{res} for $n = 1$ moves closer to the plasma boundary, and the maximum normalized beta is increased. Figure 5 shows the regions of stability with $q_s = 2.55$ and $q_s = 3.55$ for equilibria with the same pressure profile definition. The stability calculations are performed with the constant pressure damping model, with different damping coefficients. The stability limit, when expressed in terms of normalized beta, is higher at $q_s = 3.55$ than at $q_s = 2.55$ both for the resistive wall and the plasma mode. Increasing q_s to higher values further increases the stable g.

C. Mode Structure

Figures 6–8 show some eigenfunctions for equilibria that are unstable with the wall at infinity but are stabilized by a resistive wall and rotation. Figure 6 shows the radial component of the eigenfunction, $\xi_\psi = \vec{\xi} \cdot \nabla\psi$, for the ideal case with the wall at infinity.

Compare this to Fig. 7 which shows ξ_ψ for the same equilibrium surrounded by a resistive wall, but with no rotation. There is a very sharp drop in the $m = 2$ component of ξ_ψ at the $q = 2$ surface. The sharp variation of the marginal solution visible inside the $q = 2$ surface is connected with a rather small pressure gradient, so that the exponent for the "small solution" is near zero, $\nu = \sqrt{D_I} - 1/2 \approx 0.05$, at $q = 2$.

Figure 8 shows ξ_ψ and $\xi_S = \vec{\xi} \cdot (\vec{B} \times \nabla\psi)/|\nabla\psi|^2$ for an equilibrium with one rational surface ($q_s = 2.55$) with resistive wall and rotation ($|\omega_{\rm rot}/\omega_A| = 0.06$) with $\nu/\omega_A = 0.01$ for the pressure damping model. Two resonances are now visible—one inside and one outside the rational surface. The resonances are particularly distinctive in the plot of ξ_S. These resonances move away from the rational surface as $\omega_{\rm rot}$ is increased. In the lowest approximation, the Alfvén continuum frequency of a particular poloidal harmonic m and toroidal mode number n being given by $\omega_{\rm cont} = [B_0/R_0\rho^{1/2}(\psi)]|m/q(\psi) - n|$. Thus the

resonances in the $m = 2$ harmonic for this $n = 1$ mode in Fig. 8 occur at $q = 1.887$ and $q = 2.128$.

If the dissipation coefficients for the sound waves are small, the displacement exhibits sharp peaks around the surfaces resonant to the coupled Alfvén-sound continuum[21] at $\omega = \omega_{\rm rot}$. In the limit of vanishing damping coefficients and mode growth rate, these resonances approach a $1/(\psi - \psi_0)$ behavior for the parallel displacement and $\log|\psi - \psi_0|$ for the normal displacement. Larger values of the damping coefficients broaden the singularities.

IV. Wall Stabilization of Advanced Tokamak Configurations

There has been a considerable interest recently in advanced tokamak configurations,[22–25] which are usually defined as one in which the fraction of the total plasma current coming from bootstrap current is near unity, $f_{BS} \equiv I_{BS}/I_p \approx 1$, and in which there is high normalized β, $g > 3.5$, and which are mainly in the second stability region to ballooning modes. A configuration has been described,[22,23] which has a bootstrap fraction near unity, such that the bootstrap current is well aligned with the current profile, and which has large normalized β and β^*, where $\beta^* = 2\mu_0\langle p^2\rangle^{1/2}/\langle B^2\rangle$ is a measure of fusion reactivity. This configuration also has the attractive features of being completely stable to ballooning modes, and it has good stability properties to microinstabilities, such as trapped particle modes and ion temperature gradient instabilities. The configuration is characterized by high-q at the center ($q_0 = 2.5$), low-q at the edge ($q_s \approx 3.5$), and a region of negative shear in the plasma such that the minimum value of q is $q_{\rm min} \approx 2.1$. The favorable properties of this reversed shear configuration, and the procedures used to optimize it, are described in detail in Refs. 22 and 23.

This configuration, however, is unstable to low-n pressure-driven modes, which must be stabilized by a perfectly conducting wall at roughly 1.3 times the minor radius. Therefore, we have examined such equilibria to see if they can be stabilized by a resistive wall in

combination with toroidal rotation. We created a series of equilibria similar to the reverse shear equilibrium given in Ref. 23, with $q_0 = 2.5$, $q_{\min} \approx 2.2$, $q_s = 3.7$. In view of the improved wall stabilization of equilibria with more than one rational surface, shown in Fig. 5, we also examined a sequence of equilibria otherwise identical to the first, but with $q_s = 4.1$.

Results are given in Fig. 9 using both the simple pressure damping model, Eq. (6), and the parallel viscosity model, Eq. (8). For the equilibria with $q_s > 4$, both models predict a large region stable to both the plasma mode and the resistive wall mode with a suitable wall position and $\omega_{\rm rot}/\omega_A = 0.10$ up to $\beta^* \approx 5\%$. An equilibrium that is stabilized in both models with the wall at $d/a \approx 1.25$ has $q_s = 4.1$, $\beta^* = 4.7\%$, $g^* = 5.3$ (normalized β^*), $\beta_p = 2.0$, a bootstrap fraction of 0.96, and the bootstrap current well aligned with the equilibrium current. By contrast, for the equilibria with $q_s < 4$, having only one resonant surface, stabilization by the resistive wall is not very effective. The resistive wall mode is much more stable for the equilibria with two resonant surfaces (when β^* is moderately above the wall-at-infinity limit). In fact, there is a larger region of stability for $q_s > 4$ with $\omega_{\rm rot}/\omega_A = 0.05$ than for $q_s < 4$ with $\omega_{\rm rot}/\omega_A = 0.10$. It is clear from Fig. 9 that the model of the sound-wave damping affects the quantitative results, but the dependence is not dramatic.

Shown in Fig. 10 are the components ξ_ψ and ξ_S of the eigenfunction for an advanced tokamak equilibrium with one rational surface ($q_s = 3.7$). Note the resonances of the $m = 3$ harmonic and the large $m = 4$ harmonic at the edge. In Fig. 11 are the components ξ_ψ and ξ_S of the eigenfunction for an advanced tokamak equilibrium with two rational surfaces ($q_s = 4.1$). Here, there is a pair of broad resonances around the $q = 3$ surface and a somewhat sharper resonance inside the $q = 4$ surface. The resonance outside the $q = 4$ surface is in the vacuum in this case.

V. Effect of Coupling to Sound Waves

The sound waves enter the dynamics of the resistive wall mode both in the bulk of the plasma and at the continuum resonances. To quantify how strong their effect is, we made a series of stability calculations with different values of the adiabatic index: $\Gamma = 0$, 3/2 and 3 (using a fixed "parallel viscosity" term — $\pi^{1/2}|k_{||}v_{\rm thi}|v_{||}$). The result is shown in Fig. 12 as marginal d/a vs. β^* for the same equilibria as in Fig. 9. Evidently, the sound waves produce the main part of the stabilization for the resistive wall mode.

We have also made calculations in which Γ was prescribed as a function of the equilibrium flux surface. Results for the JET equilibrium with $q_s = 2.55$ are shown in Fig. 13. In this case, there is one rational surface at $q = 2$. The factor Γ was defined to fall off as a Gaussian away from the $q = 2$ surface: $\Gamma \sim \exp(-(q-2)^2/(\Delta q)^2)$. Results are shown for several values of Δq as well as for the case with no rotation, for comparison, and also the case with regular damping (Γ constant as a function of radius).

Figure 13 demonstrates that with the narrowest extent of Γ ($\Delta q = .15$) the growth rates are only slightly lower than the case with no rotation—indicating very little stabilization. Only when the radial extent of Γ is increased greatly ($\Delta q \approx 1.0$) does one see complete stabilization, but at a larger wall radius. Increasing the value of Δq further brings the curve back to the original damping case. We conclude that the stabilization of the resistive wall mode comes primarily from interaction with the sound-waves and is a bulk plasma effect.

VI. Wall Conductivity Effects

For sufficient wall conductivity, the quantitative results of the stabilization are not sensitive to the magnitude of the conductivity. The growth rates and slip frequencies are inversely proportional to the wall conductivity. However, when the wall resistivity becomes

too large, the stabilizing effects are reduced. Figure 14 shows the growth rates $\gamma\tau_w$ and the slip frequencies $\Delta\omega_{res}\tau_w$, both normalized to the wall time, for a case with the wall conductivity scaled over a range of factor 200. The values of γ and $\Delta\omega_{res}$ are normalized to the wall time, and are shown for five values of wall conductivity represented in terms of the ratio of wall time to Alfvén time τ_w/τ_A.

The normalized curves for $\tau_w/\tau_A = 4 \times 10^4$ and 4×10^5 exactly coincide. For $\tau_w/\tau_A =$ 8000 there is a slight variation in the normalized $\Delta\omega_{res} \cdot \tau_w$ curves, and in the growth rates for some values of d/a. However, at low values of d/a and near the stability threshold, the normalized growth rates are identical to those for $\tau_w/\tau_A \geq 4 \times 10^4$, resulting in the same threshold wall position for stability. When the conductivity is reduced further to $\tau_w/\tau_A = 4000$ the threshold wall position is increased, thereby reducing the size of the stability region, and it is reduced much further at $\tau_w/\tau_A = 2000$. Increasing the wall resistance such that $\tau_w/\tau_A \leq 1000$ effectively removes any wall stabilization effect.

VII. Summary

We have shown that resistive walls in combination with plasma rotation can stabilize external MHD modes leading to experimentally significant increases in the beta limit. The effect is more pronounced for broad pressure profiles and at high q_s. The wall stabilization raises the pressure limit of the low-n modes, in particular, $n = 1$. This makes the mechanism particularly attractive as ballooning modes can reach a second region of stability for large pressure and low shear, while the $n = 1$ mode does not access second stability without wall stabilization.[20] This mechanism appears to be of particular importance to advanced tokamak scenarios. Equilibria with high bootstrap fraction and negative magnetic shear in the plasma interior[22] can be stabilized with resistive walls and rotation, but not-too-low values of q at the edge (allowing for more than one rational surface) and significant rotation are needed to obtain the wall stabilization effect required in Ref. 22.

The large-aspect-ratio calculation of Eqs. (9)–(13) shows that rotation provides the stabilizing influence for the resistive wall mode and explains the counter-intuitive behavior with respect to wall position, i.e., that the mode is stable when the wall is sufficiently far away. Our calculations show that the coupling to sound waves strongly increases the stabilizing effect so that it is effective at subsonic rotation frequencies.

There is some quantitative uncertainty from modeling the the parallel motion using scalar pressure MHD with fluid dissipation terms. A kinetic description is needed in order to accurately describe this effect, and this will be the object of further study. However, all three fluid approximations used in these calculations show similar stabilizing behavior.

The numerical example with standard q-profile and broad pressure profiles shown in Fig. 2 indicates an increase in the beta limit by about 30% – 40% by the wall stabilization. Increases of similar magnitude are observed on DIII-D, and some of these are believed to be due to stabilization by the DIII-D vacuum vessel.[4] Our numerical computations show that a certain minimum rotation frequency is needed for a significant effect. For typical tokamak parameters, $\omega_{\rm rot}/\omega_A$ needs to be about 0.03 – 0.05 or larger. We note that this condition is generally satisfied in DIII-D discharges where the Alfvén frequency is typically in the range 1×10^6 s^{-1} to 2×10^6 s^{-1} and $\omega_{\rm rot}$ is between 60×10^3 s^{-1} and 200×10^3 s^{-1}.

Stabilization of reverse shear "advanced tokamak" equilibria with bootstrap fraction close to 100% and in $\beta^* \approx 5\%$ has been shown to be possible, but this requires rather high rotation velocity, close to 10% of the Alfvén speed. In these cases it is particularly important to have sufficiently high values of q_s for wall stabilization to be effective.

Acknowledgment

This research was funded in part by the Fonds National Suisse pour la Recherche Scientifique and by the European Communities under the association contracts with Switzerland and Sweden.

References

[1]F. Troyon, R. Gruber, H. Saurenmann, S. Semenzato, S. Succi, Plasma Phys. Controlled Fusion **26**, 209 (1984).

[2]E. J. Strait, Phys. Plasmas **1**, 1415 (1994).

[3]T. S. Taylor, E. A. Lazarus, M. S. Chu, J. R. Ferron, F. J. Helton, W. Howl, G. L. Jackson, T. H. Jensen, Y. Kamada, A. G. Kellman, L. L. Lao, R. J. La Haye, J. A. Leuer, J. B. Lister, T. H. Osborne, R. Snider, R. D. Stambaugh, E. J. Strait, A. D. Turnbull, in Plasma Physics and Controlled Nuclear Fusion Research 1990, Proc. 13th Int. Conf., Washington, D.C., 1990 (IAEA, Vienna, 1991), Vol. 1, p. 177.

[4]A.D. Turnbull, T.S. Taylor, E.J. Strait, S.J. Thompson, M.S. Chu, J.R. Ferron, L.L. Lao, R.T. Snider, B. Rice, D. Wròblewski, O. Sauter, paper CN-60-A-5-II-4 in Plasma Physics and Controlled Nuclear Fusion Research 1994, Proc. 15th Int. Conf., Seville, 1994 (IAEA, Vienna, 1995),

[5]D. Pfirsch and H. Tasso, Nucl. Fusion **11**, 259 (1971).

[6]Z. Yoshida and N. Inoue, Plasma Phys. Controlled Fusion **27**, 245 (1985).

[7]A. Bondeson and D. J. Ward, Phys. Rev. Lett. **72**, 2709 (1994).

[8]S. W. Haney and J. P. Freidberg, Phys. Fluids **B1**, 1637 (1989), Sec. V.

[9]C. G. Gimblett, Nucl. Fusion **26**, 617 (1986).

[10]L. E. Zakharov and S. V. Putvinskii, Sov. J. Plasma Phys. **13**, 68 (1987).

[11]A. Bondeson and M. Persson, Nucl. Fusion **28**, 1887 (1988).

[12]T. H. Jensen and M. S. Chu, J. Plasma Phys. **30**, 57 (1983).

[13]J. Finn, "Resistive Wall Stabilization of External Kinks and Tearing Modes," submitted to Phys. Plasmas, (1994).

[14]A. Bondeson, G. Vlad, and H. Lütjens, Phys. Fluids **B4**, 1899 (1992).

[15]D. J. Ward, S. C. Jardin, and C. Z. Cheng, J. Comp. Phys. **104**, 221 (1993).

[16]C. Z. Cheng and M. S. Chance, J. Comp. Phys. **71**, 124 (1987).

[17]A. Bondeson and R. Iacono, Phys. Fluids **B1**, 1431 (1989).

[18]G. W. Hammett and F. W. Perkins, Phys. Rev. Lett. **64**, 3019 (1990).

[19]F. Waelbroeck and L. Chen, Phys. Fluids **B3**, 601 (1991).

[20]A. Bondeson, in Proc. 20th EPS Conf. on Controlled Fusion and Plasma Physics (European Physical Society, Geneva 1993), Part IV, p. 1339.

[21]C. Z. Cheng and M. S. Chance, Phys. Fluids **29**, 3695 (1986).

[22]C. Kessel, J. Manickam, G. Rewoldt, and W. M. Tang, Phys. Rev. Lett. **72**, 1212 (1994).

[23]J. Manickam, M. S. Chance, S. C. Jardin, C. Kessel, D. Monticello, N. Pomphrey, A. Reiman, C. Wang, and L. E. Zakharov, Phys. Plasmas **1**, 1601 (1994).

[24]P. A. Politzer, T. Casper, C. B. Forest, P. Gohil, W. W. Heidbrink, A. W. Hyatt, R. A. James, R. Jong, L. L. Lao, M. Makowski, W. Meyer, G. D. Porter, G. T. Sager, B. W. Stallard, H. St. John, S. J. Thompson, A. D. Turnbull, D. Wròblewski, Phys. Plasmas **1**, 1545 (1994).

[25]"Optimized Profiles for Improved Confinement and Stability in the DIII-D Tokamak," T. S. Taylor and the DIII-D Team, to appear in Plasma Phys. and Control. Fusion **36**, (1994).

Figures

FIG. 1. Growth rate $\gamma_{\rm res}$ and slip frequency $\Delta\omega_{\rm res} = \omega_{\rm rot} - \omega_{\rm res}$ of resistive wall mode, both normalized to the wall time τ_w, and growth rate of plasma mode $\gamma_{\rm ideal}$ versus wall radius for $n = 1$ mode with g about 30% above free-boundary limit. This graph was calculated using the Hammett-Perkins[18] approximation, Eq. (7), with $\chi = 2/\pi$.

FIG. 2. Marginal wall position versus Troyon factor g for the plasma (ideal) and resistive wall modes (resistive) with toroidal mode numbers $n = 1$ and $n = 2$. The plasma mode is stable for $d < d_{\rm ideal}$ and the resistive wall mode for $d > d_{\rm res}$. The region stable to both the $n = 1$ and $n = 2$ modes is bounded by the $n = 1$ resistive wall mode and the $n = 2$ plasma mode.

FIG. 3. Marginal wall distance versus Troyon factor g for the plasma mode (marked "ideal") and the resistive wall mode using different fluid approximations for the damping of the sound waves. Curves (a)–(e) apply for $|\omega_{\rm rot}/\omega_A| = 0.06$. (a)–(b) give results for the pressure damping model Eq. (7) with (a) $\nu/\omega_A = 0.025$ and (b) $\nu/\omega_A = 0.0025$. (c)–(e) give results for the parallel viscosity model Eq. (8) with (c) $\kappa = 0.1$, (d) $\kappa = 0.885$, and (e) $\kappa = 1.77$. Also shown is one curve with half the rotation frequency, $|\omega_{\rm rot}/\omega_A| = 0.03$, with the same damping model as in (e).

FIG. 4. Growth rate versus wall position for several different values of rotation velocity. The solid symbols are the growth rates with the given rotation velocity, and the open symbols are with a resistive wall but no rotation.

FIG. 5. Marginal wall distance versus Troyon factor g for equilibria with the same pressure profile, with $q_s = 2.55$ and $q_s = 3.55$. (a)–(b) are the resistive wall modes for $q_s = 2.55$ with the pressure damping model, Eq. (6), with (a) $\nu/\omega_A = 0.025$ and (b) $\nu/\omega_A = 0.0025$. (c)–(d) are resistive wall modes for $q_s = 3.55$ equilibria with (c) $\nu/\omega_A = 0.025$ and (d) $\nu/\omega_A = 0.01$.

FIG. 6. Radial component ξ_ψ of the eigenfunction as a function of $s = \sqrt{\psi}$ for the ideal instability (wall at infinity).

FIG. 7. Radial component ξ_ψ of the eigenfunction for the same equilibrium as in Fig. 6, but with a surrounding resistive wall with no rotation.

FIG. 8. Components ξ_ψ (a) and ξ_S (b) of the eigenfunction for the same equilibrium as in Fig. 6 with a resistive wall and rotation, $|\omega_{\rm rot}/\omega_A| = 0.06$, with damping factor $\nu/\omega_A = 0.025$.

FIG. 9. Stability boundaries for equilibria with negative central shear and high bootstrap fraction. Results are shown for sequences with $q_s = 3.7$ (dashed curves) and $q_s = 4.1$ (unbroken curves). The ideal $n = 1$ boundaries are given by the solid squares, the $n = 1$ resistive wall mode boundaries using the parallel viscosity model (viscosity), Eq. (2), and $|\omega_{\rm rot}/\omega_A| = 0.10$ are given by the open circles, while the simple pressure damping model (p. d. m.) results are the open triangles. The crosses represent the resistive wall mode boundary using the parallel viscosity model for the $q_s = 4.1$ sequence at half the rotation speed, $|\omega_{\rm rot}/\omega_A| = 0.05$.

FIG. 10. Components ξ_ψ (a) and ξ_S (b) of the eigenfunction for the advanced tokamak configuration with one rational surface, $q_s = 3.7$. Here, the simple pressure damping model, Eq. (6), is used with rotation velocity of $|\omega_{\rm rot}/\omega_A| = 0.10$ and damping factor $\nu/\omega_A = 0.10$.

FIG. 11. Components ξ_ψ (a) and ξ_S (b) of the eigenfunction for the advanced tokamak configuration with two rational surfaces, $q_s = 4.1$. The parameters are otherwise identical to the case of Fig. 10.

FIG. 12. Marginal wall position for different values of the adiabatic index Γ. The equilibrium is the same as in Fig. 9, $|\omega_{\rm rot}/\omega_A| = 0.10$ and the parallel viscosity model was used.

FIG. 13. Growth rates γ_{res} of the resistive wall mode vs. wall position d/a for $|\omega_{rot}/\omega_A| = 0.06$ with Γ varied as a Gaussian function around the $q = 2$ surface with width Δq. Also shown, for comparison, are the growth rates for the case with no rotation (open squares), and also the case (solid squares) with regular damping (Γ constant as a function of radius).

FIG. 14. Growth rates γ_{res} (a) and slip frequencies $\Delta\omega_{res} = \omega_{rot} - \omega_{res}$ (b), normalized to the wall time, τ_w, vs. wall position, d/a, for several values of wall conductivity. The curves correspond to wall times normalized to the Alfvén time $\tau_w/\tau_A = 2000$ to $\tau_w/\tau_A = 4 \times 10^5$.

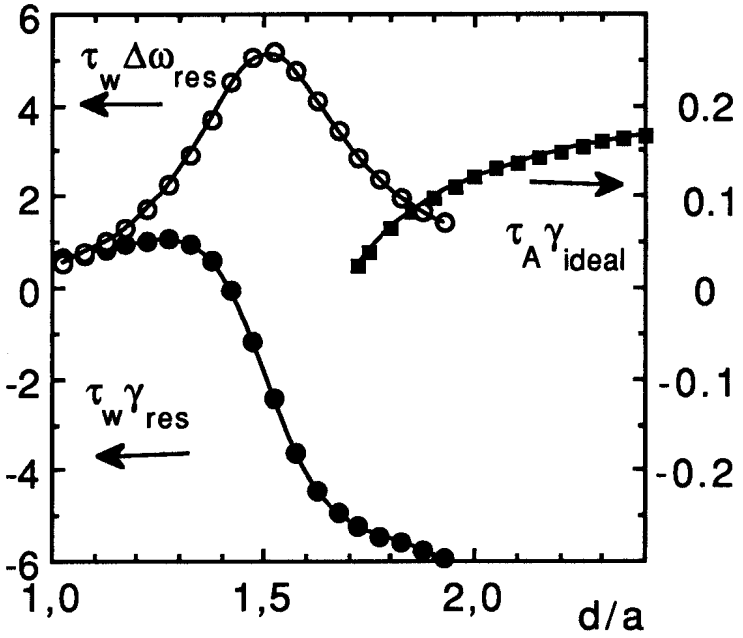

Figure 1

Figure 2

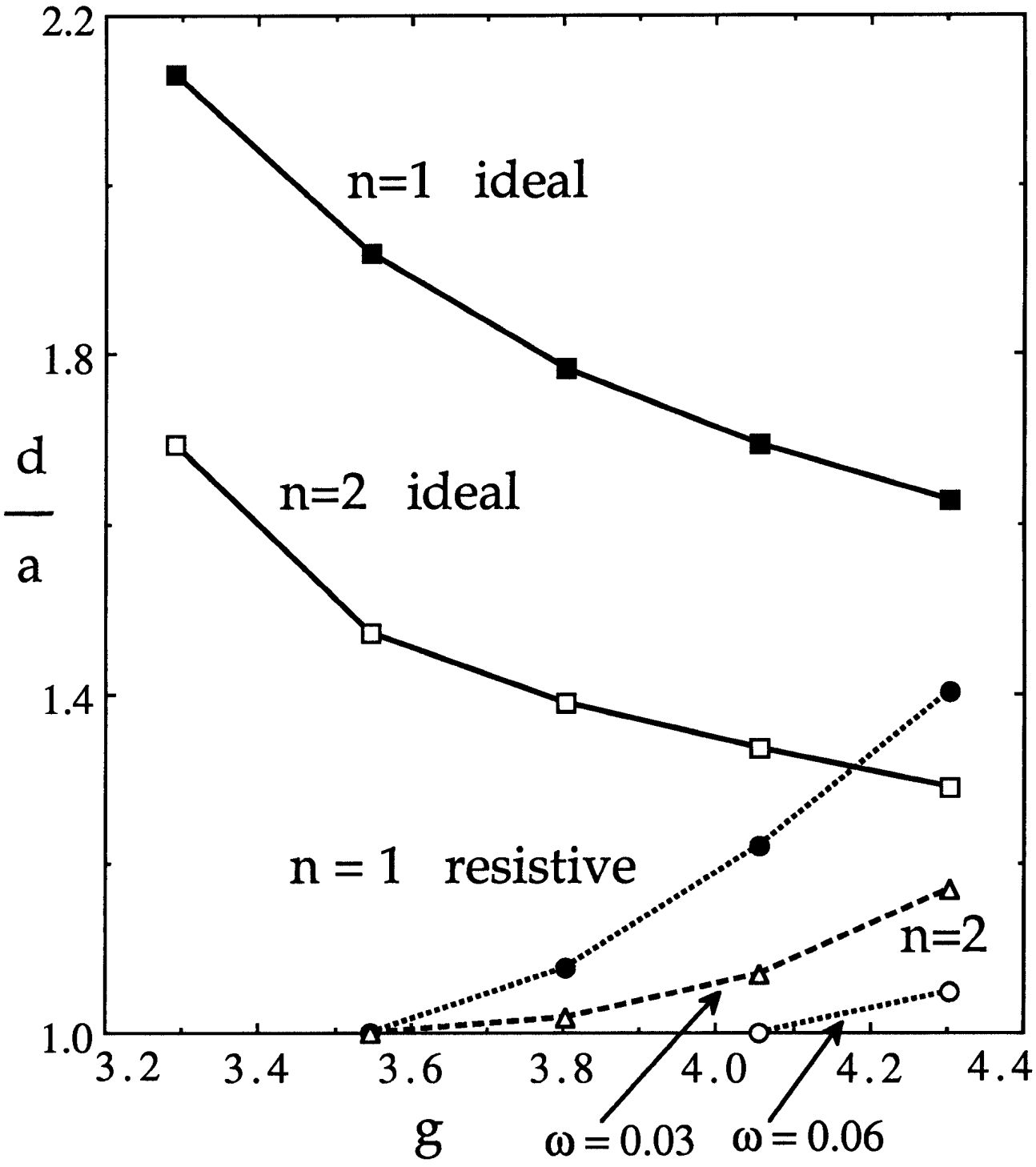
2.2
1.8
1.4
1.0
d/a
n=1 ideal
n=2 ideal
n = 1 resistive
n=2
3.2
3.4
3.6
3.8
4.0
4.2
4.4
g
ω = 0.03
ω = 0.06

Figure 3

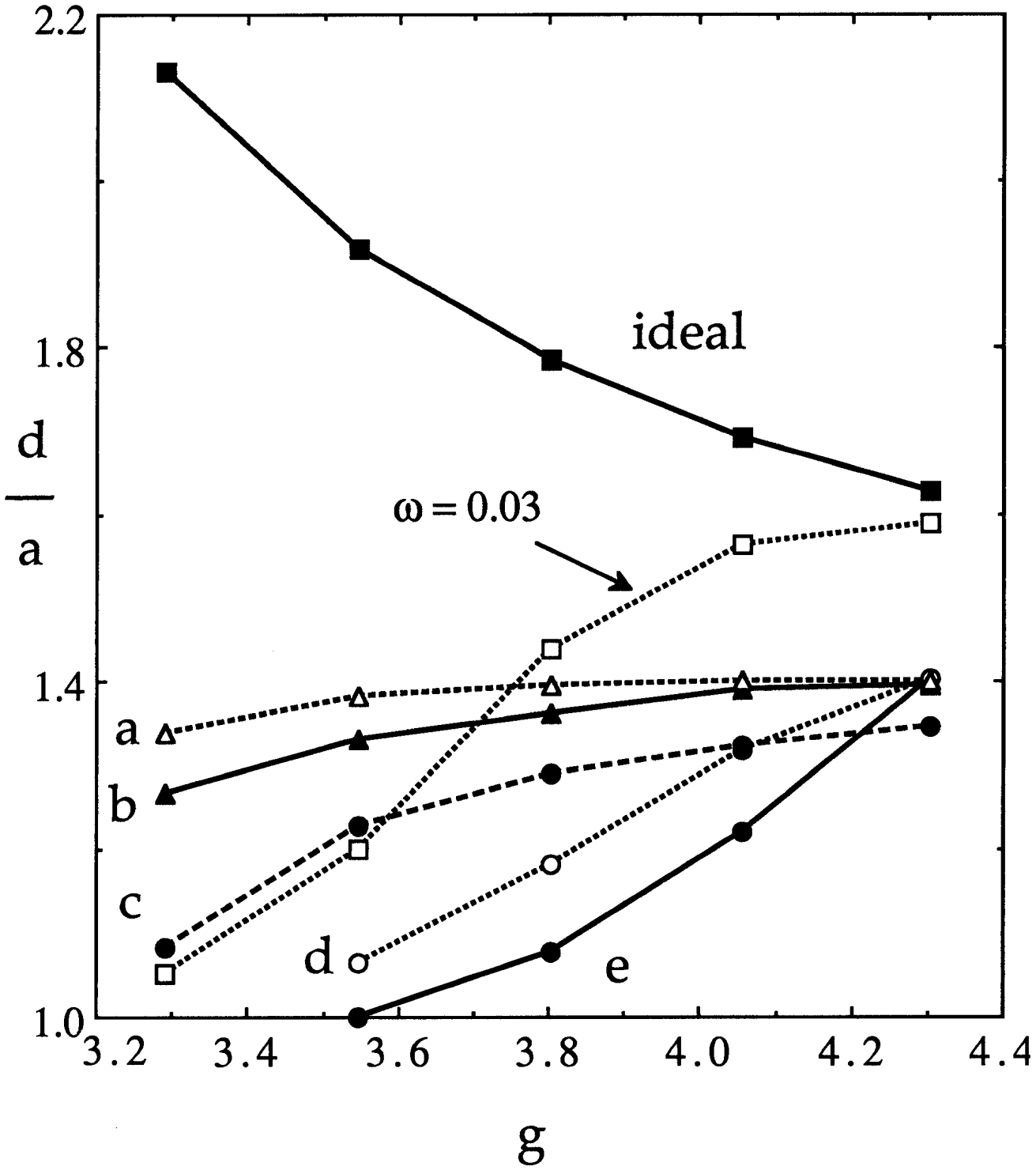

Figure 4

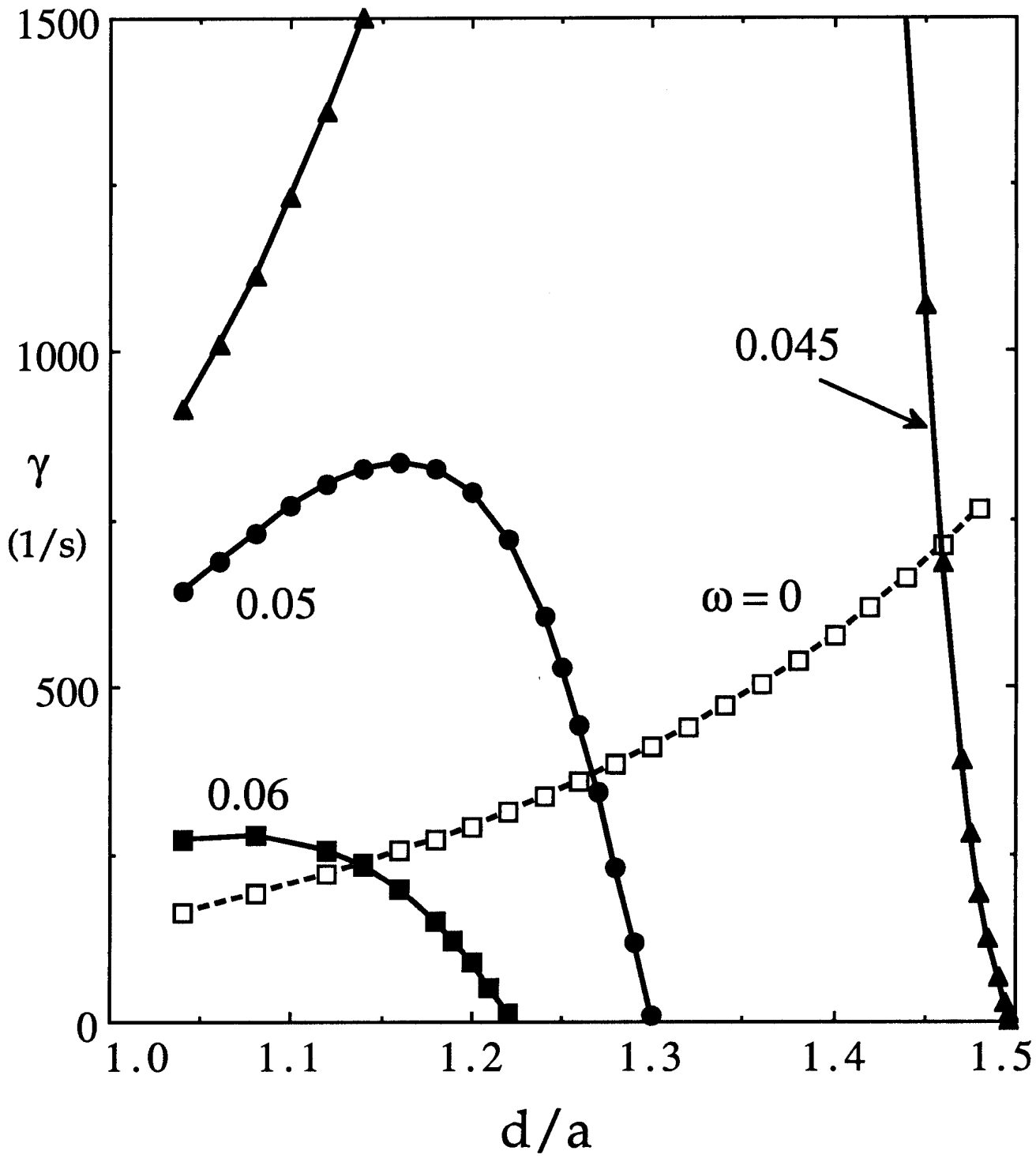

Figure 5

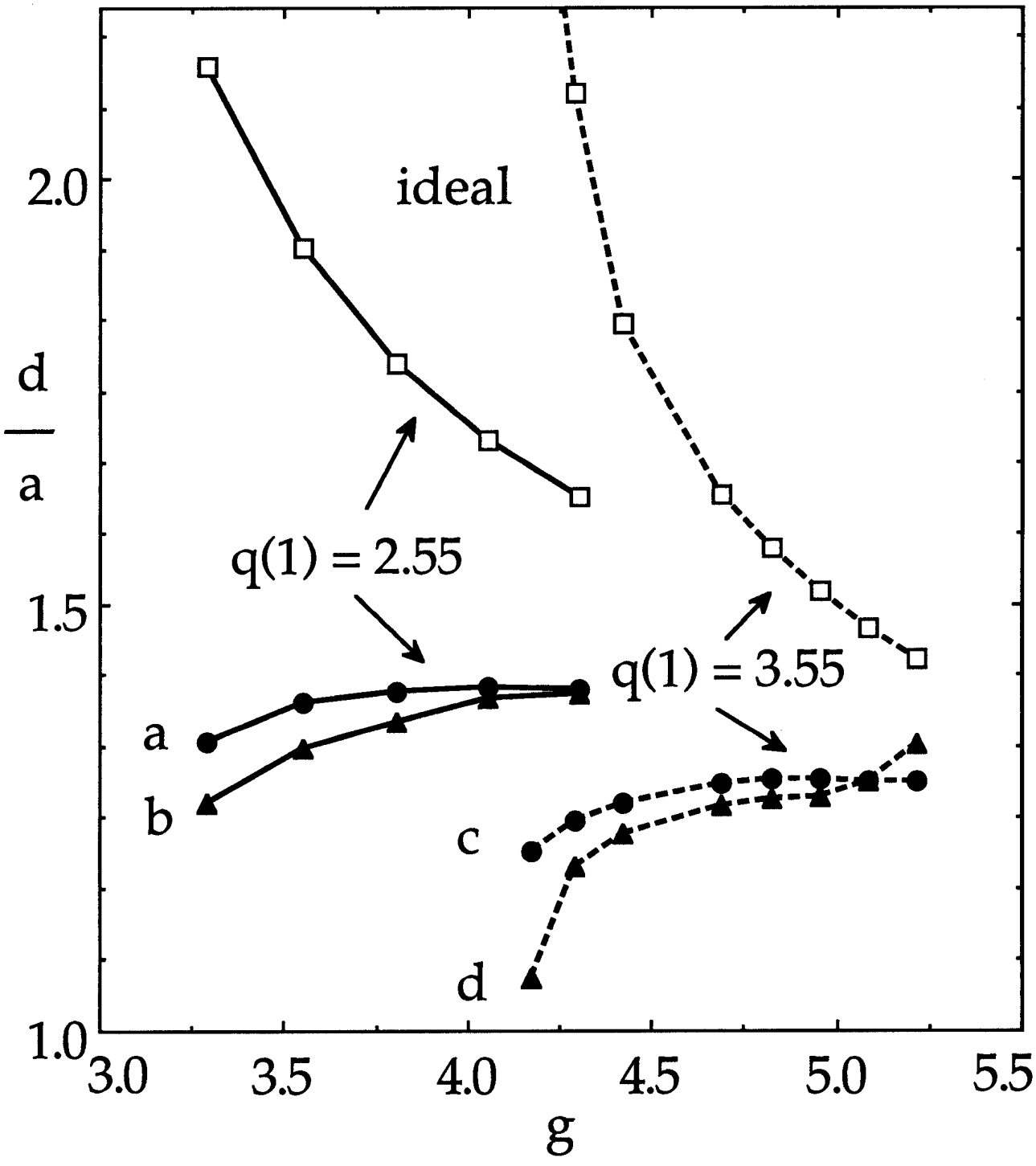

Figure 6

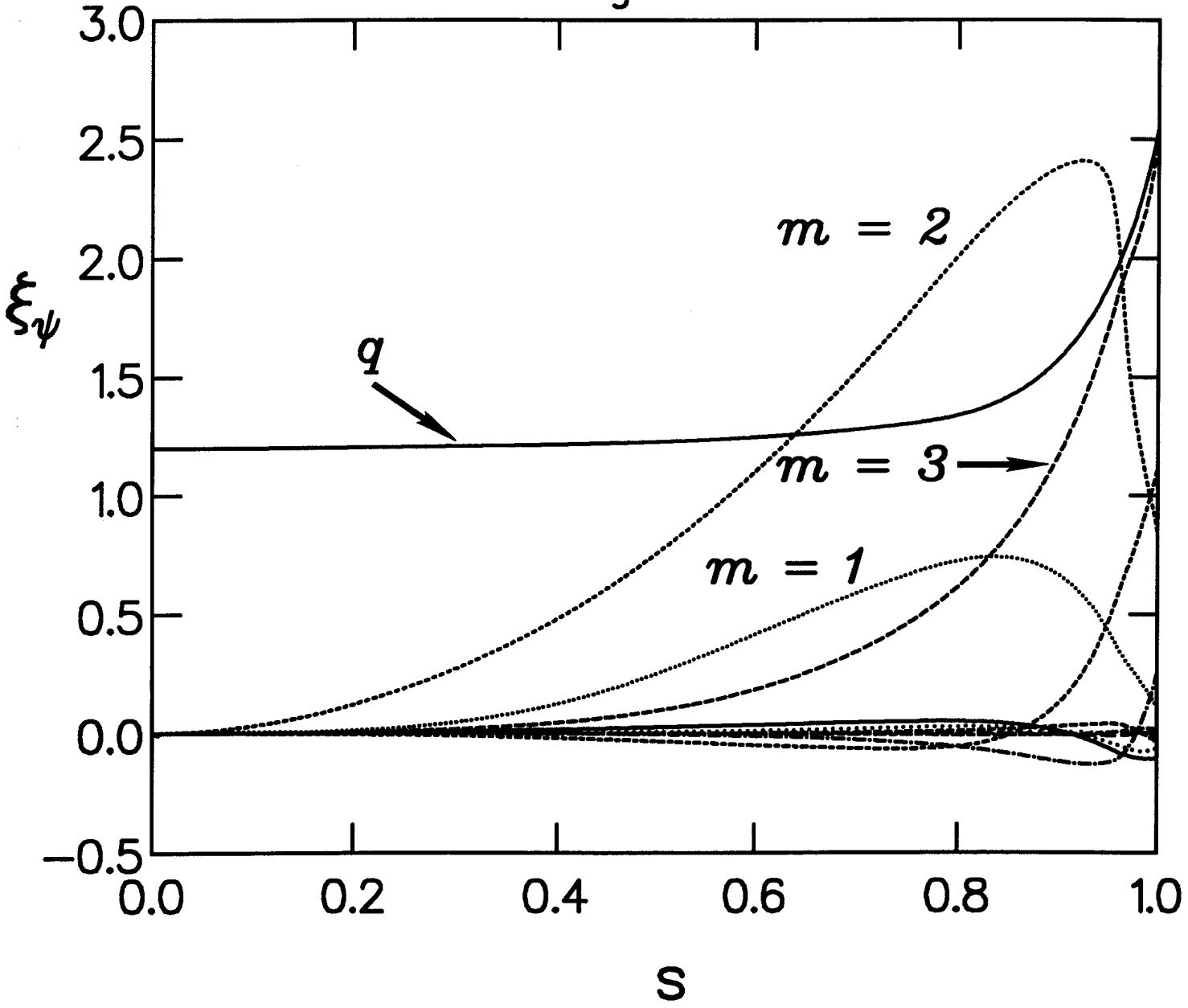

Figure 7

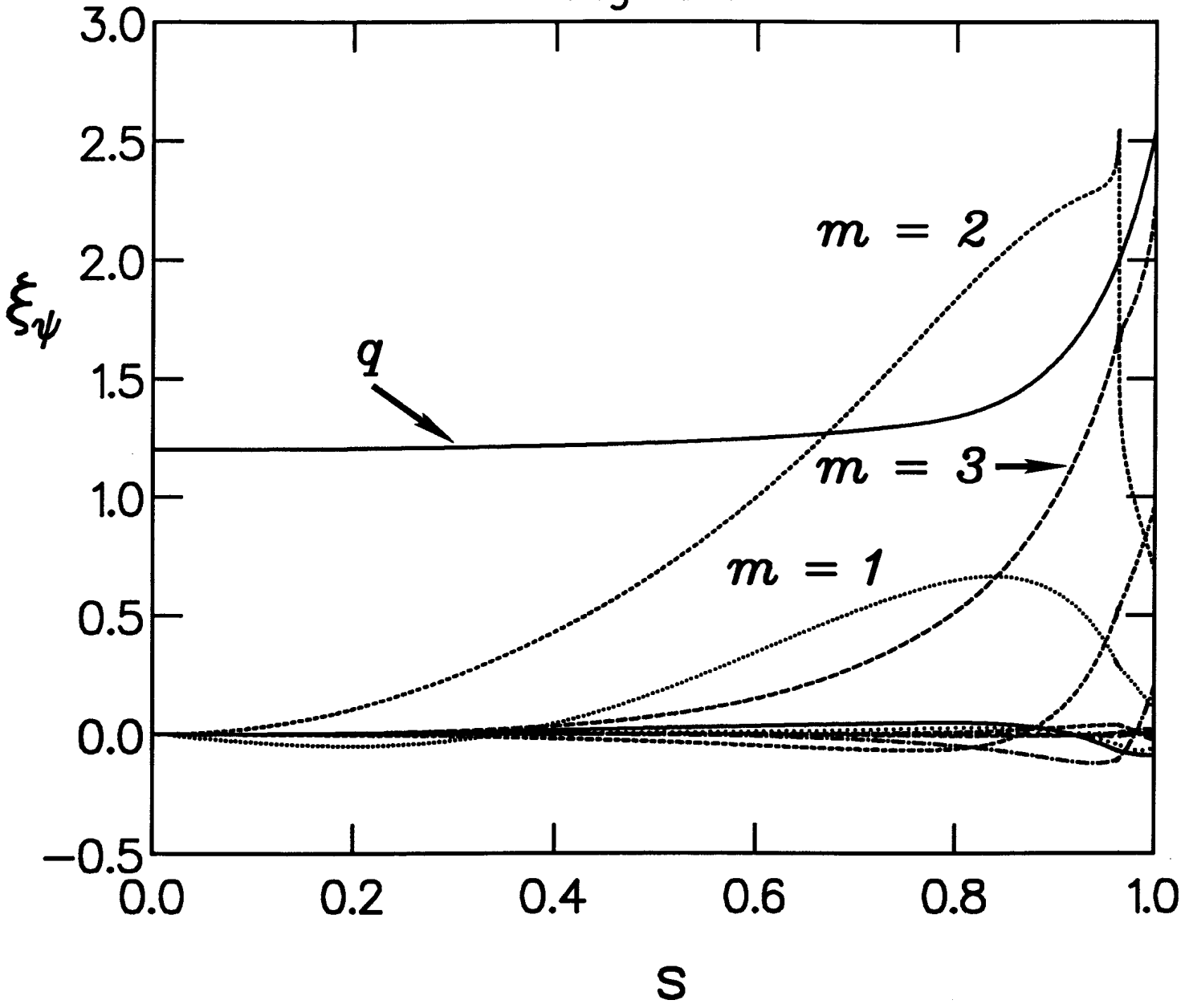

Figure 8 (a)

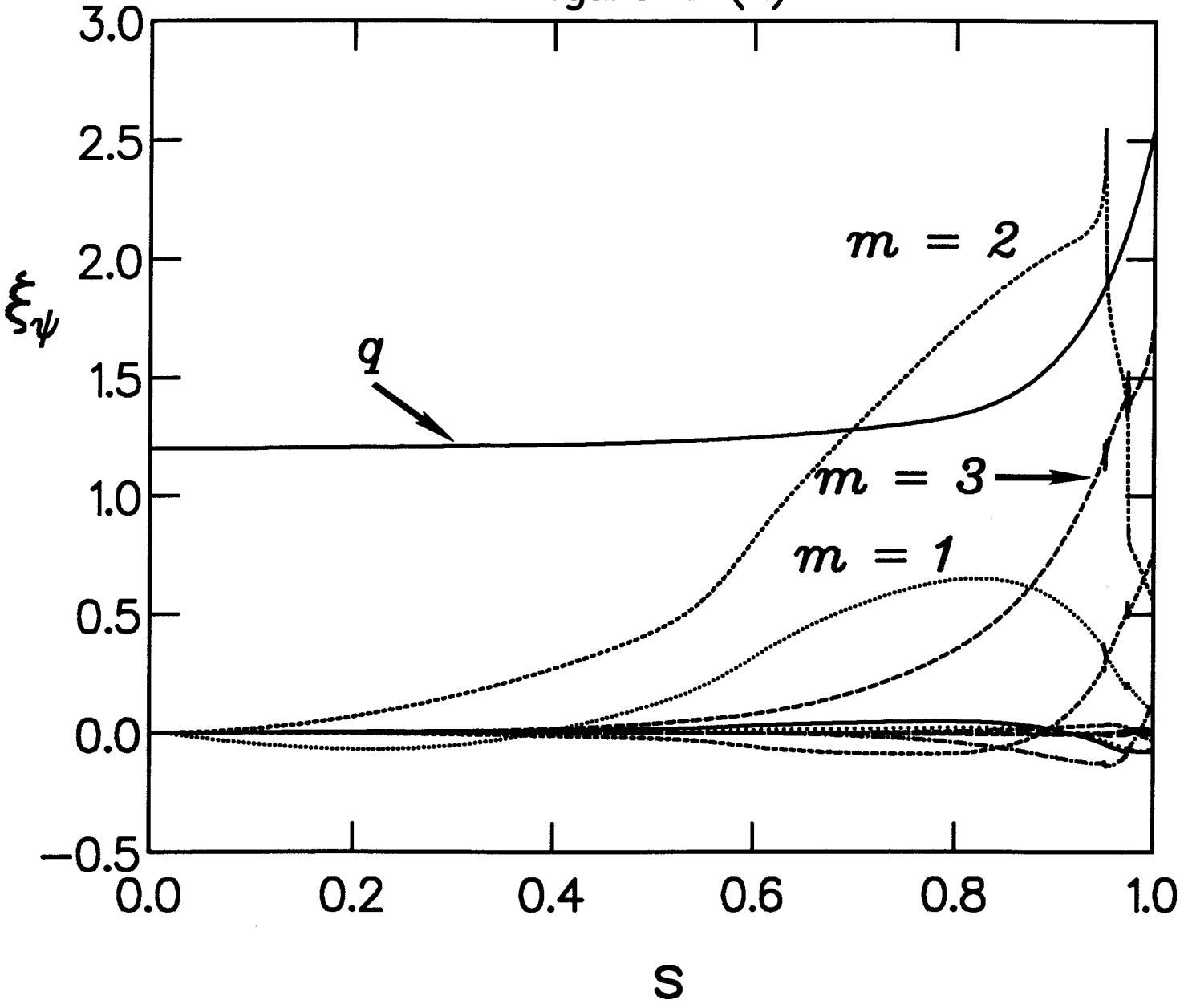

Figure 8 (b)

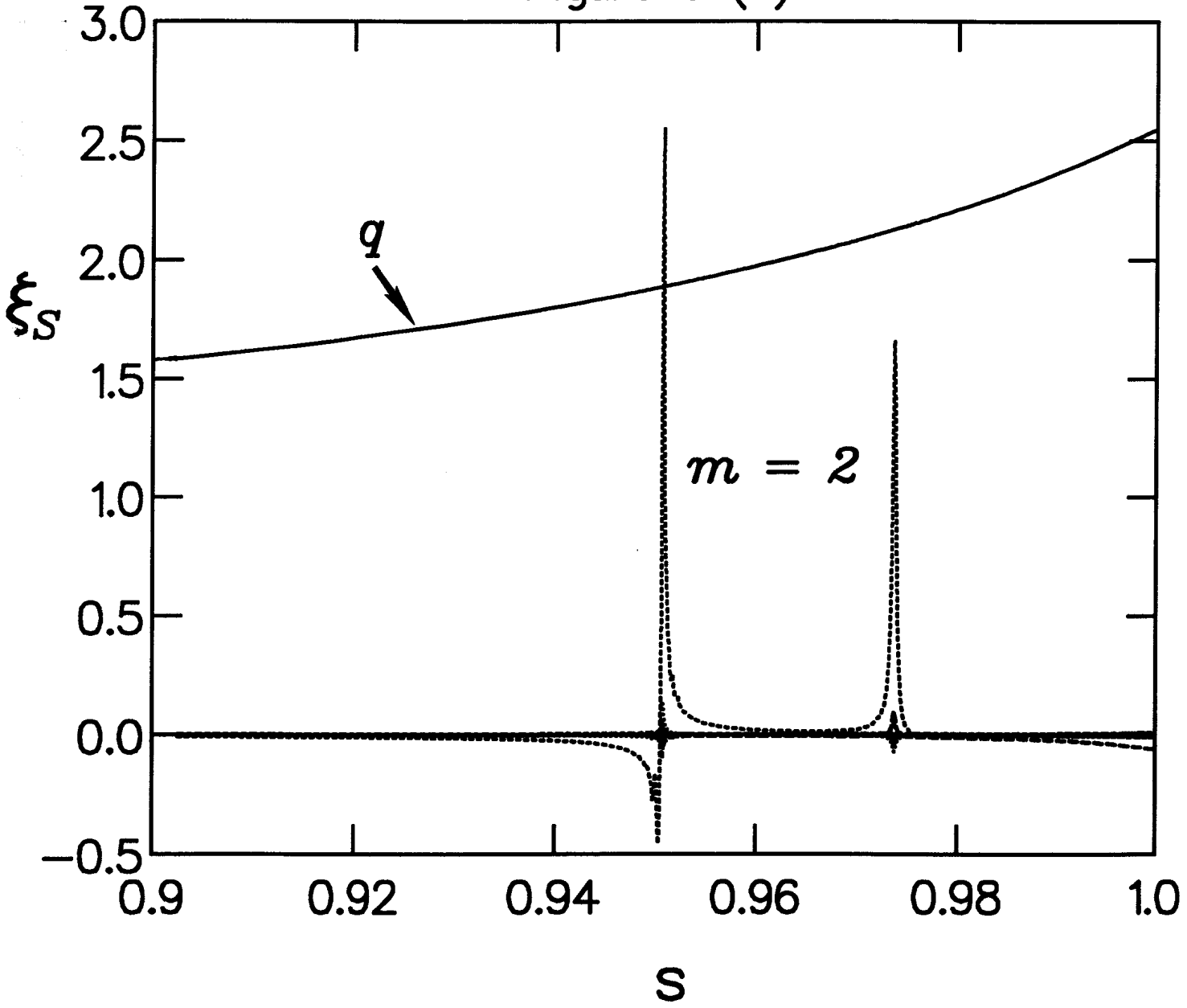

Figure 9

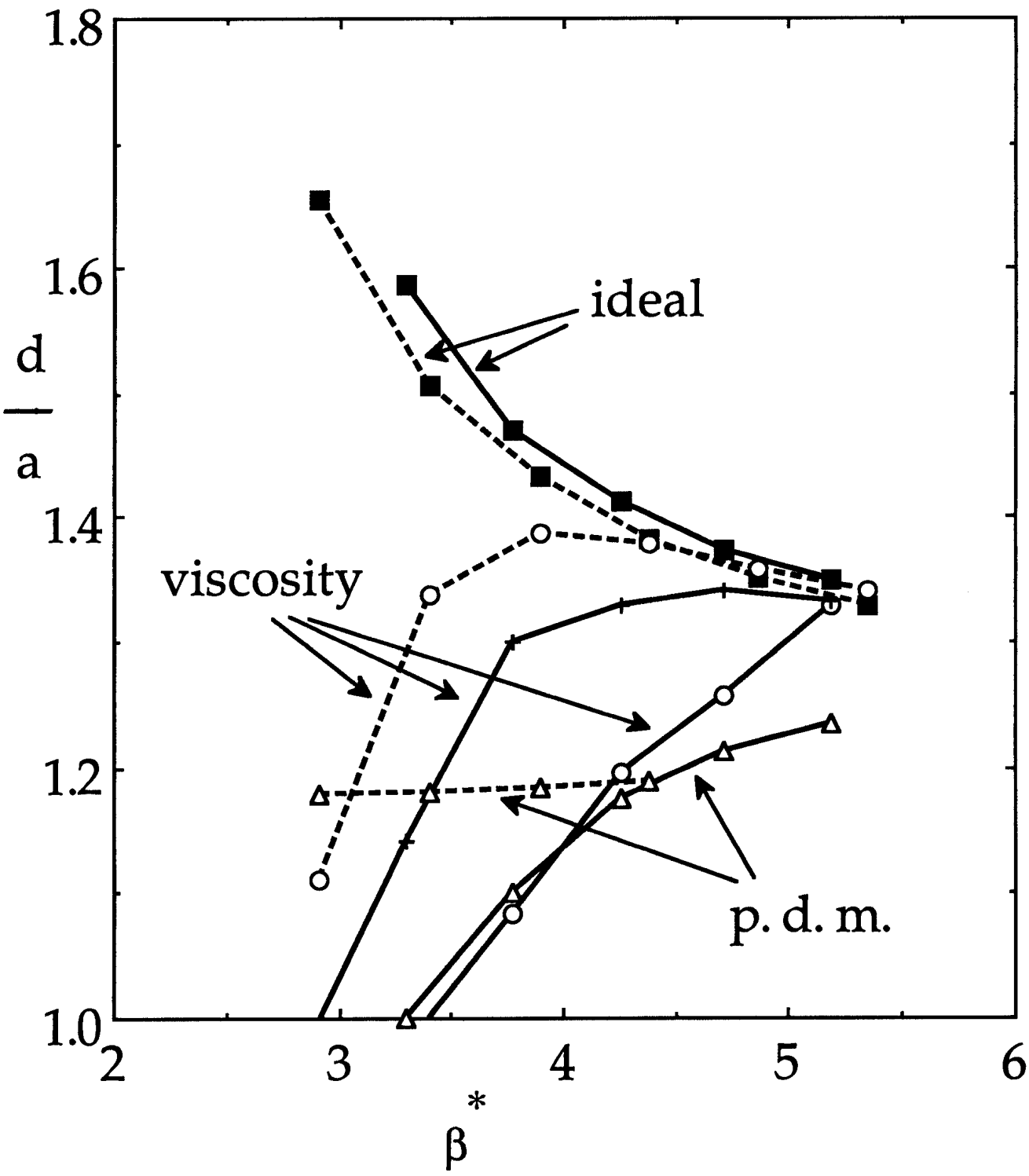

Figure 10 (a)

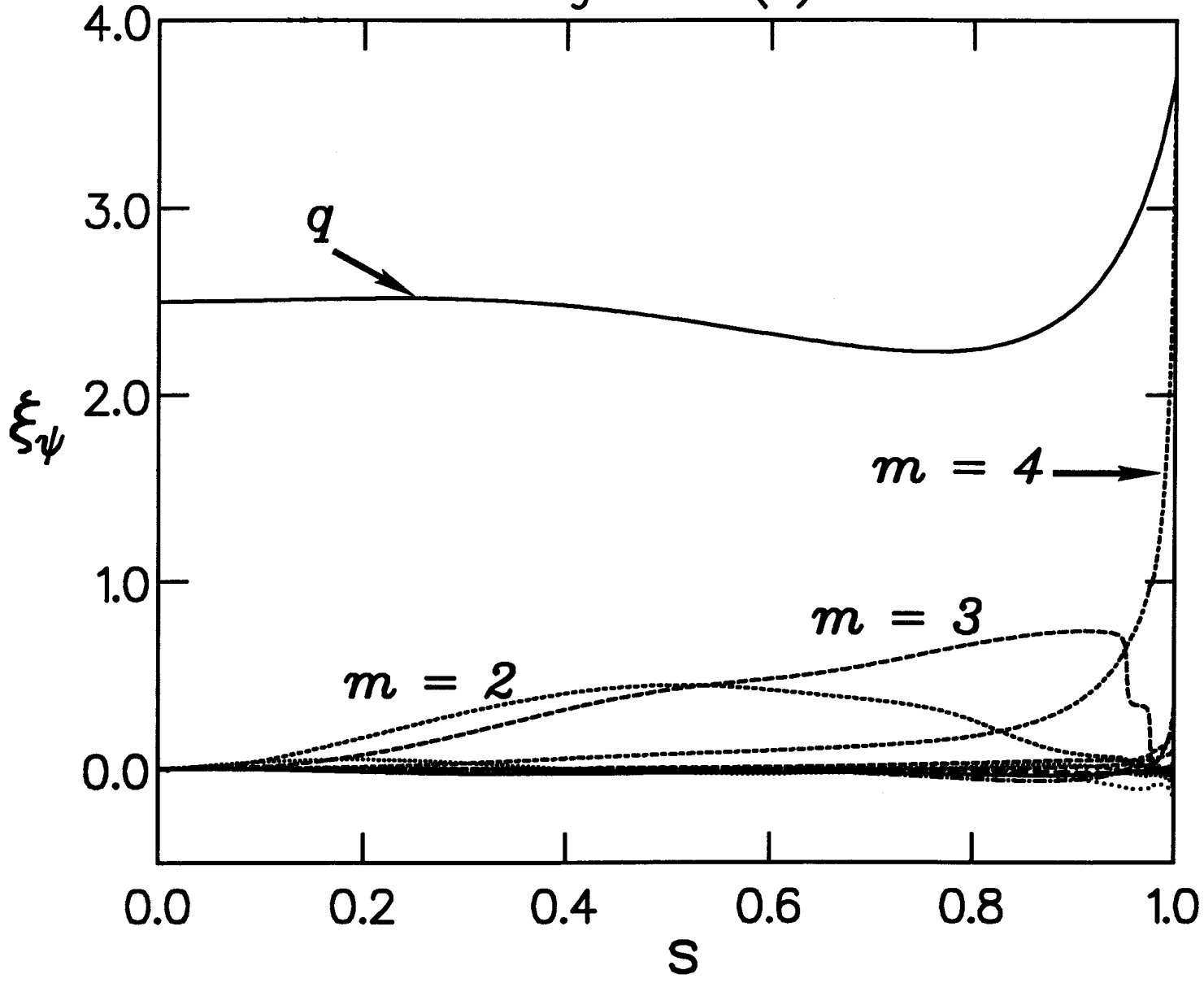

Figure 10 (b)

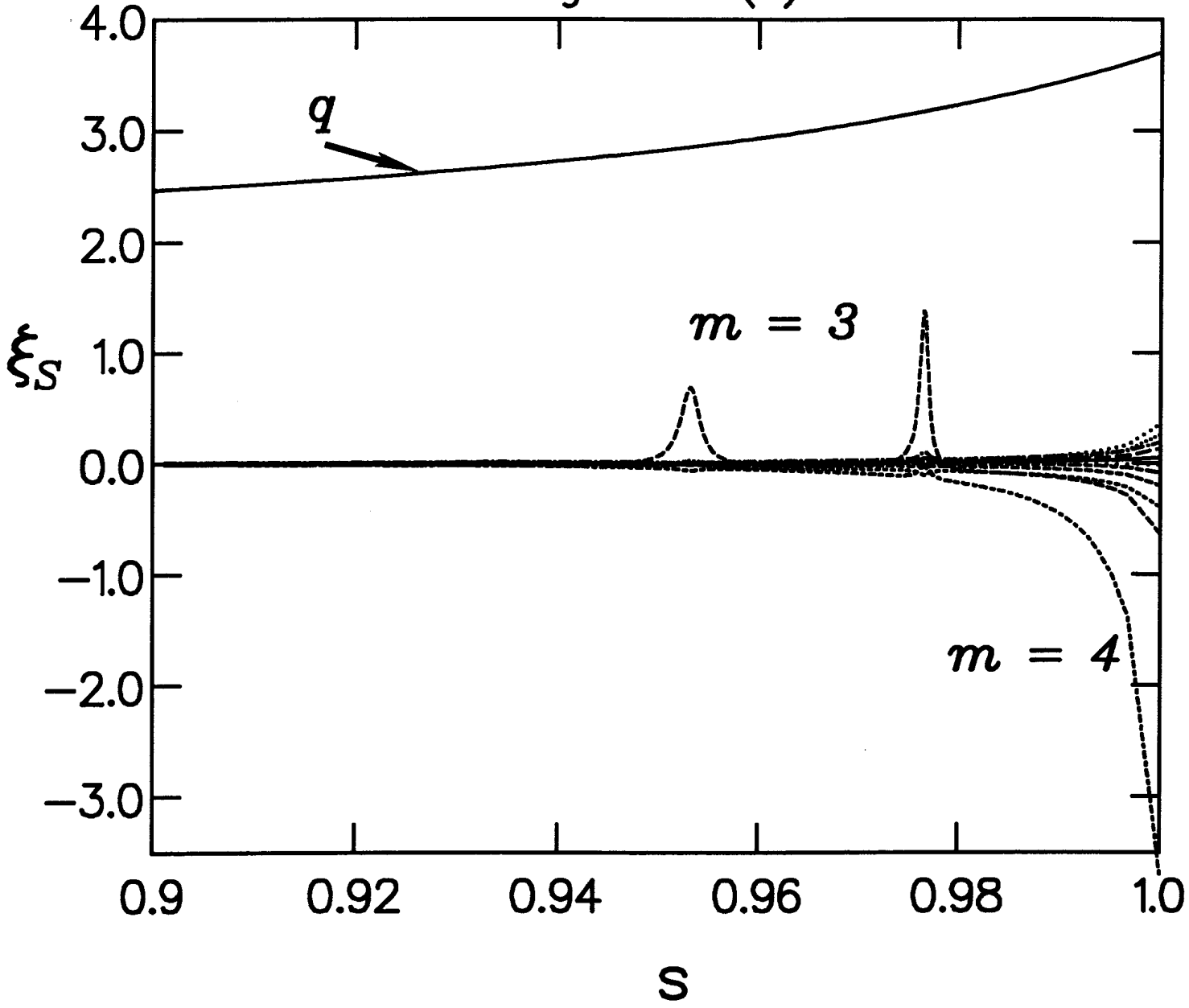

Figure 11 (a)

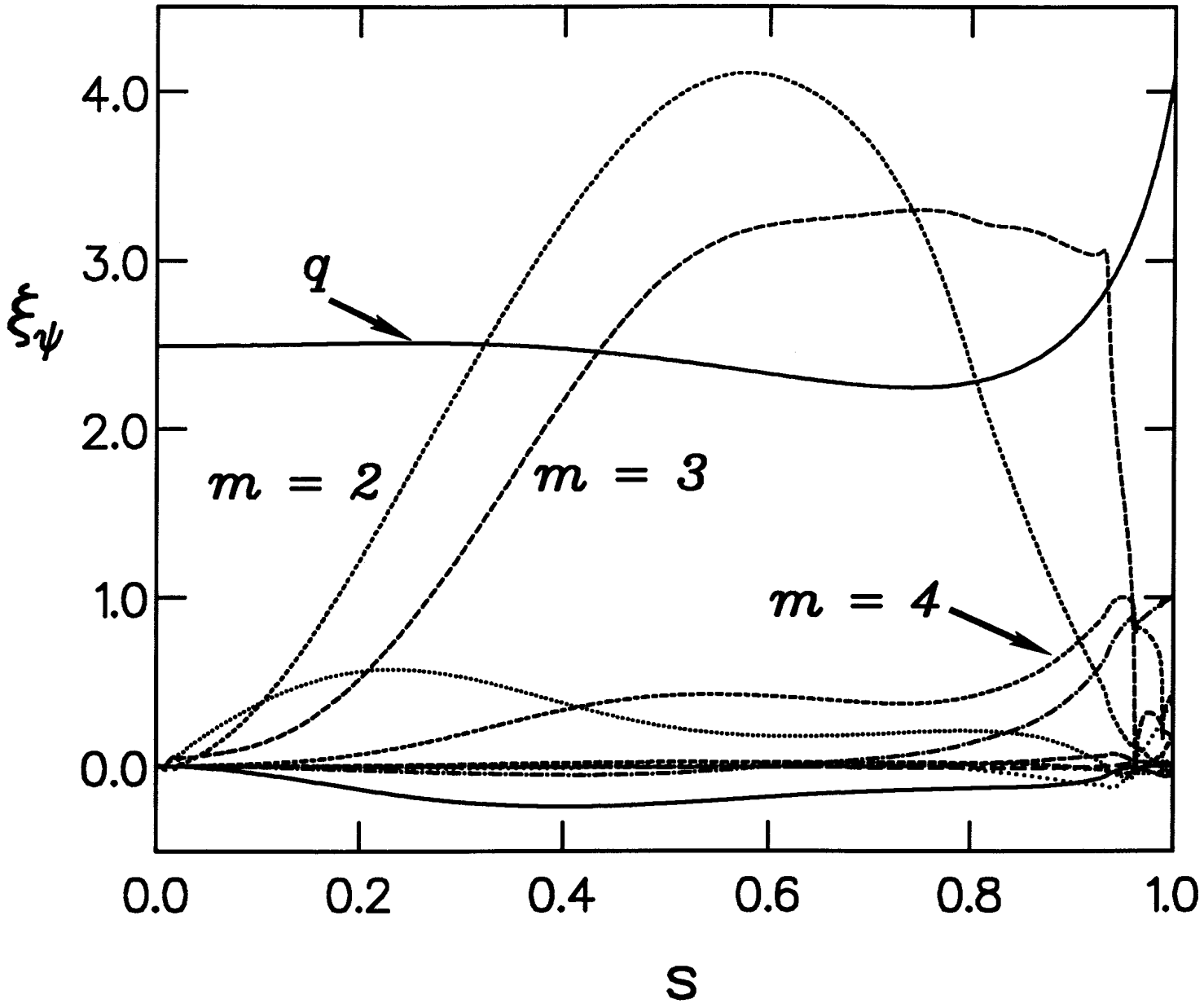

Figure 11 (b)

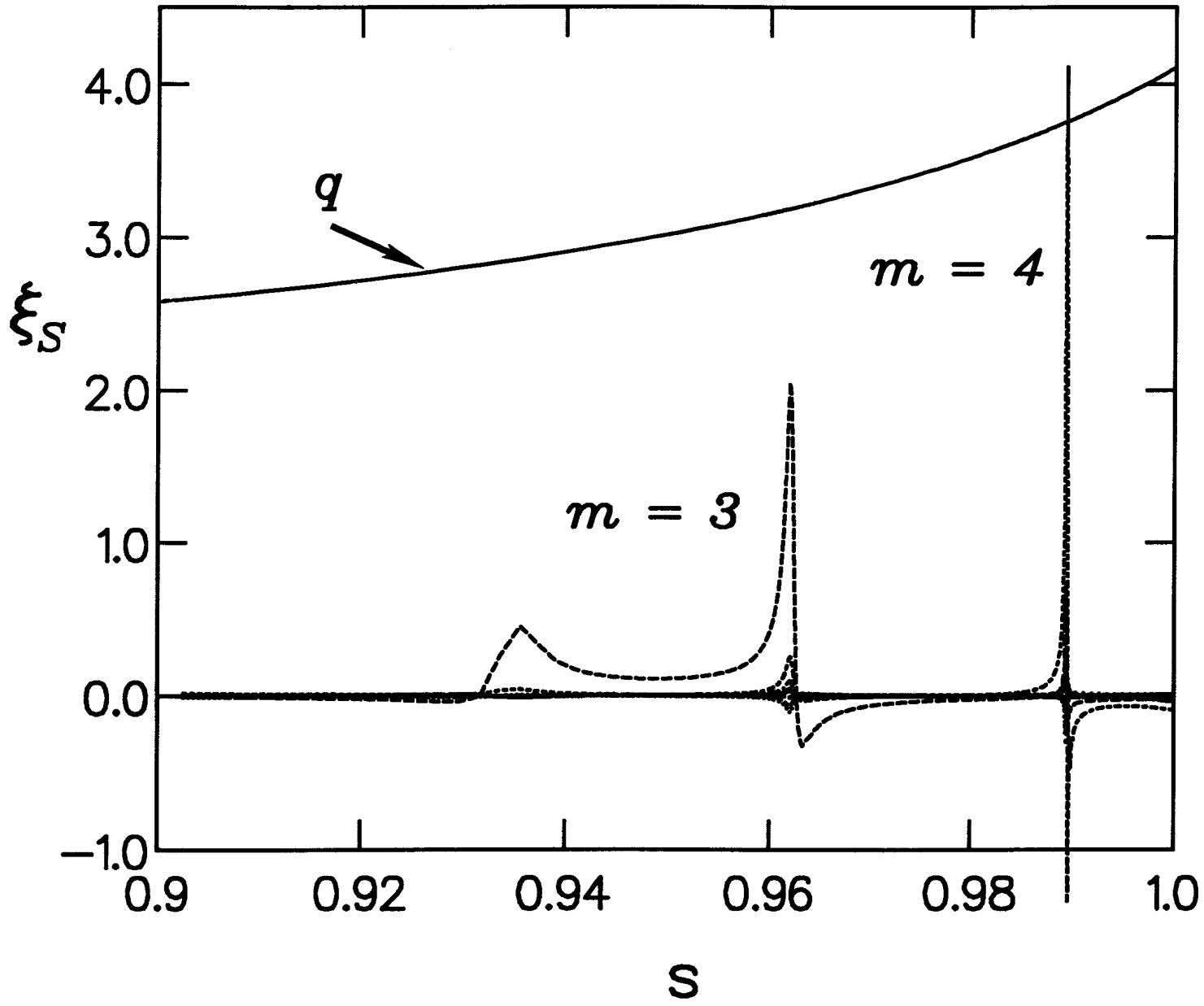

Figure 12

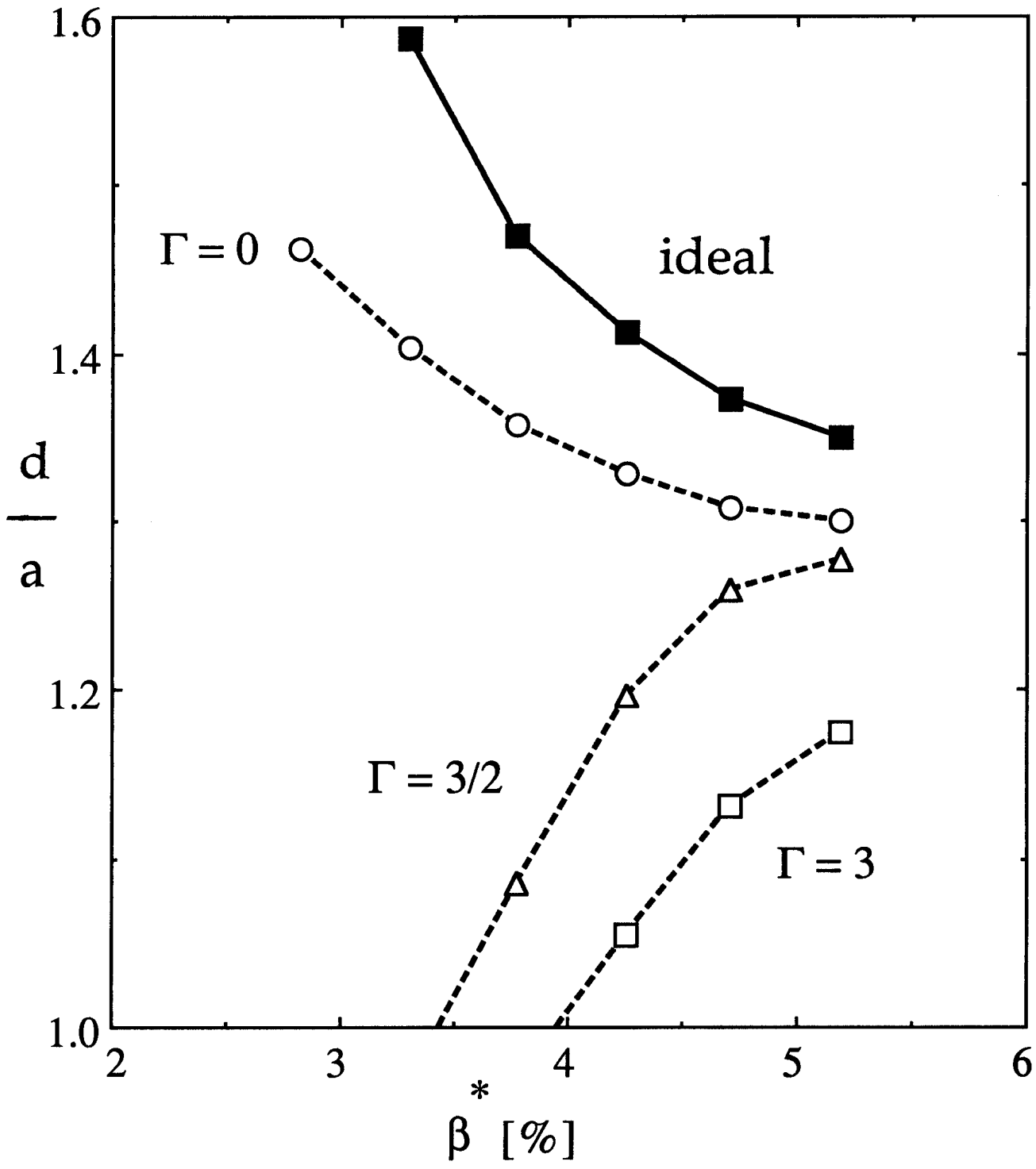

Figure 13

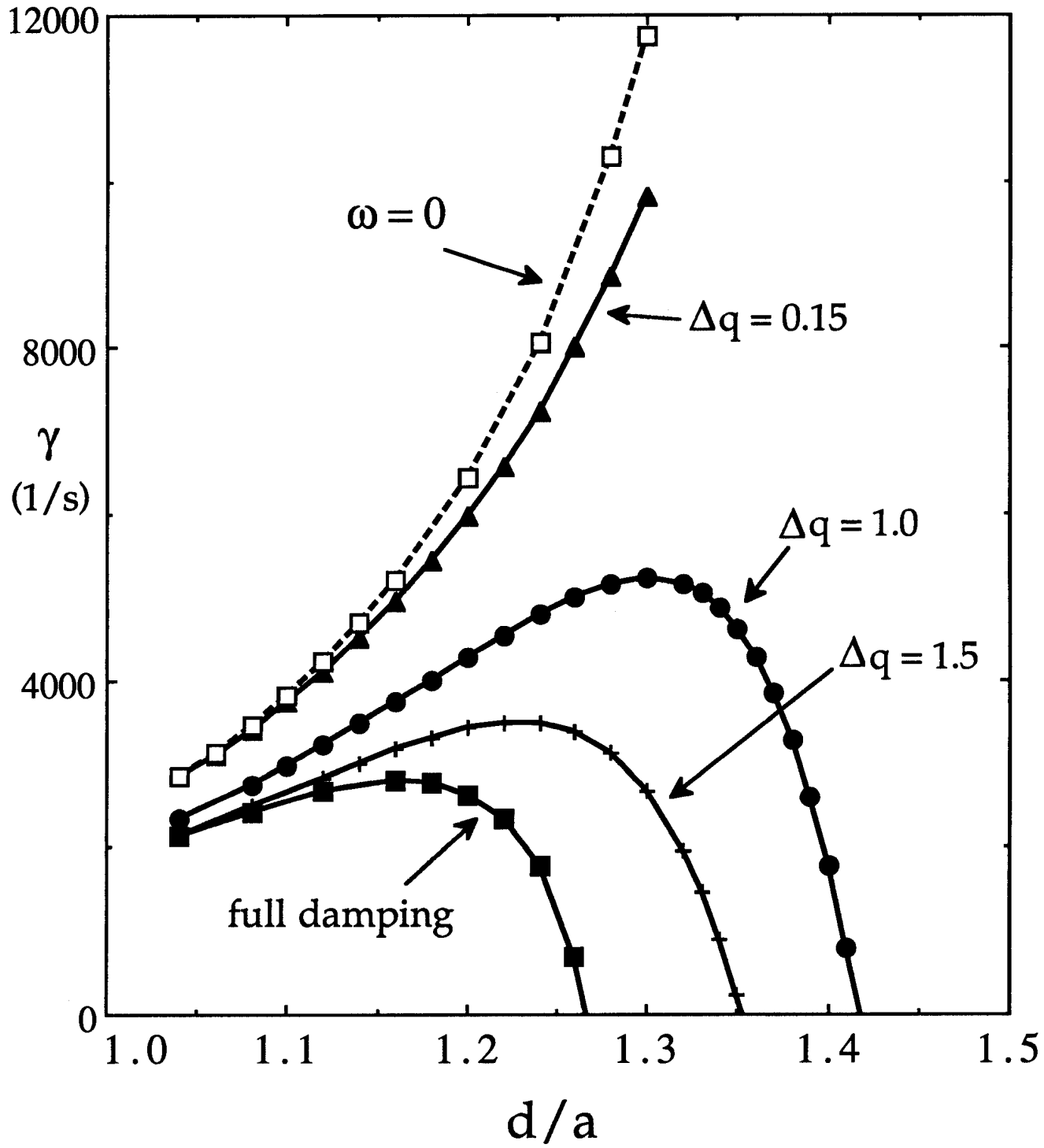
12000
8000
4000
0
γ
(1/s)
ω = 0
Δq = 0.15
Δq = 1.0
Δq = 1.5
full damping
1.0
1.1
1.2
1.3
1.4
1.5
d/a

Figure 14 (a)

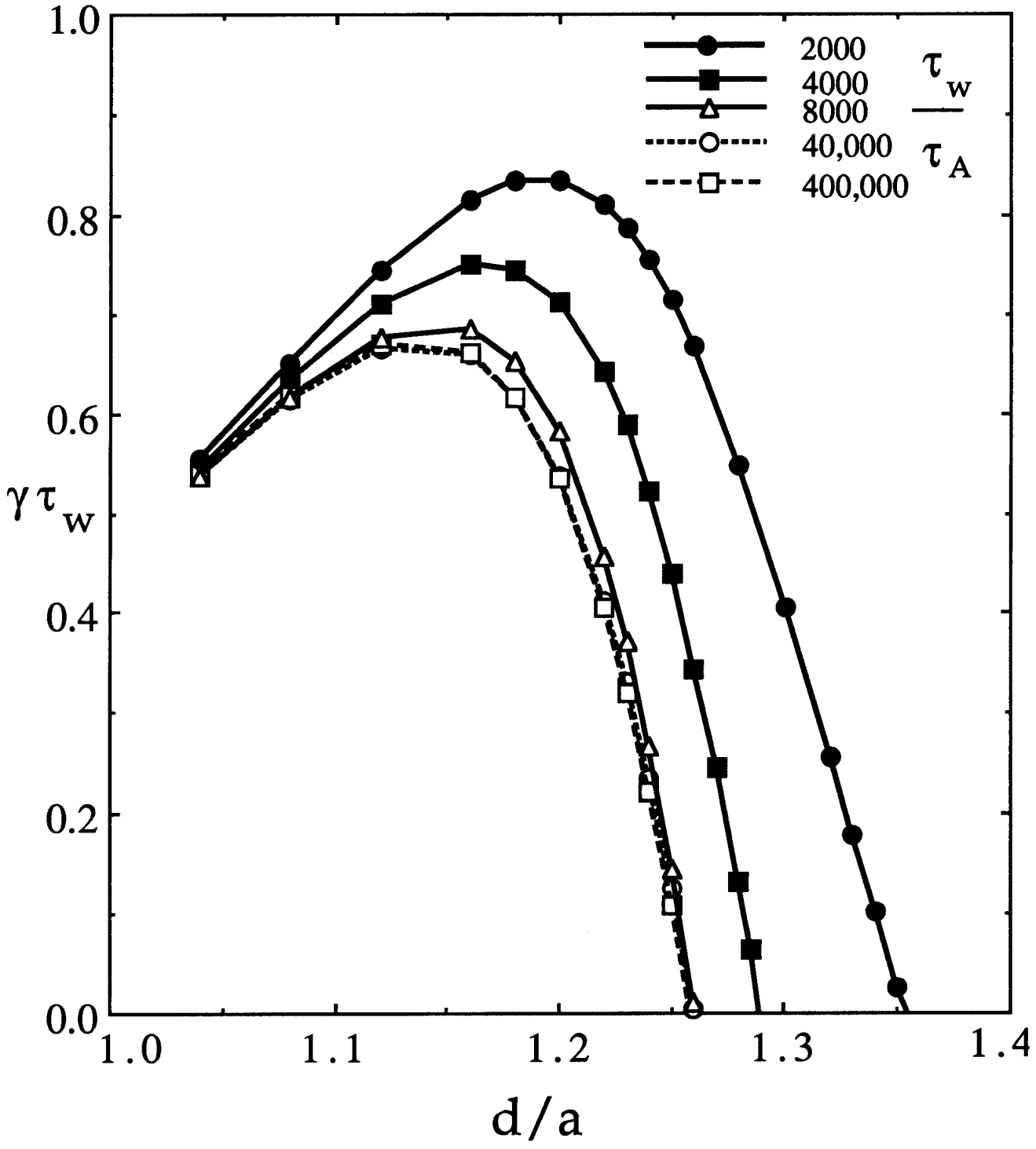
1.0
0.8
0.6
0.4
0.2
0.0
γτw
1.0
1.1
1.2
1.3
1.4
d/a
2000
4000
8000
40,000
400,000
τw
τA

Figure 14 (b)

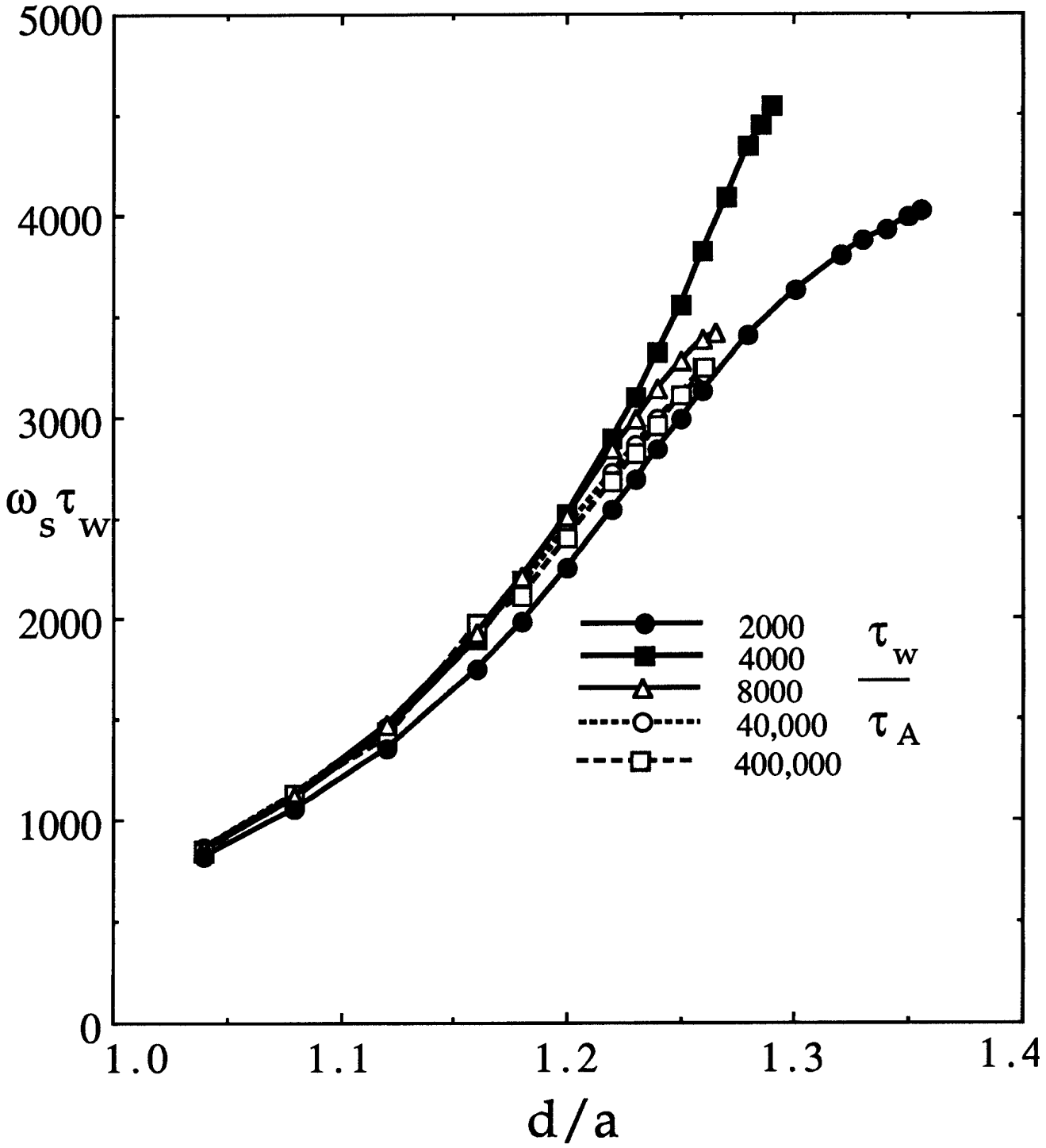
5000
4000
3000
2000
1000
0
$\omega_s \tau_w$
1.0
1.1
1.2
1.3
1.4
d/a
2000
4000
8000
40,000
400,000
$\frac{\tau_w}{\tau_A}$